



Open Archive Toulouse Archive Ouverte (OATAO)

OATAO is an open access repository that collects the work of some Toulouse researchers and makes it freely available over the web where possible.

This is an author's version published in: <https://oatao.univ-toulouse.fr/26944>

Official URL : <https://doi.org/10.2514/1.C035509>

To cite this version :

Sgueglia, Alessandro and Schmollgruber, Peter and Bartoli, Nathalie and Bénard, Emmanuel and Morlier, Joseph and Jasa, John and Martins, Joaquim R. R. A. and Hwang, John T. and Gray, Justin S. Multidisciplinary Design Optimization Framework with Coupled Derivative Computation for Hybrid Aircraft. (2020) Journal of Aircraft, 57 (4). 715-729. ISSN 0021-8669

Any correspondence concerning this service should be sent to the repository administrator:

tech-oatao@listes-diff.inp-toulouse.fr

Multidisciplinary Design Optimization Framework with Coupled Derivative Computation for Hybrid Aircraft

Alessandro Sgueglia,^{*} Peter Schmollgruber,[†] and Nathalie Bartoli[‡]

ONERA/DTIS–University of Toulouse, 31055 Toulouse, France

Emmanuel Benard[§]

ISAE-SUPAERO, Université de Toulouse, France

Joseph Morlier[¶]

University of Toulouse, 31055 Toulouse, France

John Jasa^{**} and Joaquim R. R. A. Martins^{††}

University of Michigan, Ann Arbor, Michigan 48109

John T. Hwang^{‡‡}

University of California San Diego, La Jolla, California 92093

and

Justin S. Gray^{§§}

NASA John H. Glenn Research Center, Cleveland, Ohio 44139

<https://doi.org/10.2514/1.C035509>

Hybrid-electric aircraft are a potential way to reduce the environmental footprint of aviation. Research aimed at this subject has been pursued over the last decade; nevertheless, at this stage, a full overall aircraft design procedure is still an open issue. This work proposes to enrich the procedure for the conceptual design of hybrid aircraft found in literature through the definition of a multidisciplinary design optimization (MDO) framework aimed at handling design problems for such kinds of aircraft. The MDO technique has been chosen because the hybrid aircraft design problem shows more interaction between disciplines than a conventional configuration, and the classical approach based on multidisciplinary design analysis may neglect relevant features. The procedure has been tested on the case study of a single-aisle aircraft featuring hybrid propulsion with distributed electric ducted fans. The analysis considers three configurations (with 16, 32, and 48 electric motors) compared with a conventional baseline at the same 2035 technological horizon. To demonstrate the framework's capability, these configurations are optimized with respect to fuel and energy consumption. It is shown that the hybrid-electric concept consumes less fuel/energy when it flies on short range due to the partial mission electrification. When one increases the design range, penalties in weight introduced by hybrid propulsion overcome the advantages of electrified mission segment: the range for which hybrid aircraft have the same performance of the reference conventional aircraft is named the “breakdown range.” Starting from this range, the concept is no longer advantageous compared to conventional aircraft. Furthermore, a tradeoff between aerodynamic and propulsive efficiency is detected, and the optimal configuration is the one that balances these two effects. Finally, multiobjective optimization is performed to establish a tradeoff between airframe weight and energy consumption.

Nomenclature

| | | |
|-------------------------|---|---|
| AR | = | aspect ratio |
| b | = | span |
| C_D | = | drag coefficient |
| $C_{D_{eq}}$ | = | trim drag coefficient |
| C_{D_i} | = | induced drag coefficient |
| C_{D_w} | = | wave drag coefficient |
| C_{D_0} | = | drag coefficient at zero lift |
| C_L | = | lift coefficient |
| c_r | = | root chord |
| c_t | = | tip chord |
| \mathbf{c}_{CCM} | = | vector containing the certification's specification |
| E_c | = | energy consumption |
| e | = | specific energy density |
| f, g, h, l | = | generic function |
| k_e | = | Oswald coefficient |
| L/D | = | lift-to-drag ratio |
| l_{nac} | = | nacelle length |
| $\mathcal{M}_{takeoff}$ | = | rotational momentum at takeoff |
| m_f | = | fuel mass |
| \mathcal{N} | = | yaw momentum |
| N_b | = | number of batteries |
| N_{EM} | = | number of engines |
| P | = | power |
| p | = | specific power density |
| R | = | range |

^{*}Ph.D. Candidate, 2 avenue Edouard Belin; also ISAE-SUPAERO, 10 avenue Edouard Belin, 31055 Toulouse, France; alessandro.sgueglia@onera.fr.

[†]Research Engineer, Information Processing and Systems Department; peter.schmollgruber@onera.fr. Member AIAA.

[‡]Senior Researcher, Information Processing and Systems Department; nathalie.bartoli@onera.fr. Member AIAA.

[§]Professor in Aircraft Design, DCAS; e.benard@isae.fr. Member AIAA.

[¶]Professor in Structural Mechanics; also ICA, ISAE-SUPAERO, MINES ALBI, UPS, INSA, CNRS, 3 rue Caroline Aigle, 31400 Toulouse, France; j.morlier@isae.fr. Member AIAA.

^{**}Ph.D. Candidate, Department of Aerospace Engineering; johnjasa@umich.edu. Member AIAA.

^{††}Professor of Aerospace Engineering, Department of Aerospace Engineering, Fellow AIAA.

^{‡‡}Assistant Professor, Department of Mechanical and Aerospace Engineering; jhwang@eng.ucsd.edu. Member AIAA.

^{§§}Aerospace Engineer, Propulsion System Analysis Branch; justing.s.gray@nasa.gov. Member AIAA.

| | | |
|----------------|---|---|
| t/c | = | thickness-to-chord ratio |
| V | = | velocity |
| w_f | = | fuselage width |
| x | = | position along the x axis |
| \mathbf{x} | = | design variables vector |
| y_k | = | wing break section |
| α | = | parameter, varying between zero and one |
| η | = | efficiency |
| Λ_{25} | = | sweep angle, at 25% of the chord |
| λ | = | taper ratio |
| τ | = | volume |

Subscripts

| | | |
|-----|---|-----------------|
| app | = | approach |
| b | = | battery |
| cs | = | cooling system |
| g | = | generator |
| HT | = | horizontal tail |
| toc | = | top of climb |
| ts | = | turboshaft |
| VT | = | vertical tail |
| w | = | wing |

I. Introduction

IN RECENT years, the aviation industry has been facing constraints due to growing air traffic: without any action, its environmental footprint will be unsustainable.[†] To reduce the impact of aviation, disruptive changes at the aircraft level are required. Fostered by the progress made in the automotive industry, significant efforts have been achieved in promoting hybrid and electric concepts [1], coupled with new technologies such as distributed propulsion for thrust generation [2,3] and boundary-layer ingestion (BLI) technology [4,5]. Distributed propulsion is a technology that has gained attention in past years because it can increase the propulsive efficiency through the reduction of fan pressure ratios [2,6,7]. Distributed propulsion is particularly well suited to electric aircraft because it is easier to distribute electric motors, as evidenced by its use in the NASA X-57 [8–13] and the NASA N3-X hybrid wing–body concepts [14–17]. BLI ingests the boundary layer from the aircraft wing or fuselage to increase the aerodynamic efficiency [18,19]. These two technologies are related and can enhance each other [3].

The main issue when dealing with a new conceptual aircraft is that most of the aircraft design methods used for conventional configurations are no longer applicable. Even the basic Breguet equation has to be modified to take into account an electric power source, both on its own or coupled with another one [20,21]. On a more complex level, hybrid-electric aircraft have more possible interactions between disciplines than a conventional aircraft [22–24]. As an example, thermal aspects play a key role in this kind of architecture and are a driver for the overall design, whereas they have no impact on a conventional aircraft [12,25].

In the last few years, research has been focusing on the problem of defining a preliminary design sizing process. Isikveren et al. [26] developed a set of strategies to deal with dual-energy aircraft in a general way, without focusing on the sources themselves. Pernet et al. [27] and Cinar et al. [28] presented a modified design process that includes hybrid-electric propulsion to evaluate aircraft performance. Ludowicy et al. [29] performed comparative studies between different configurations for a light aircraft with serial distributed propulsion. De Vries et al. [30,31] developed a preliminary design process that estimates the aeropropulsive effects in a distributed propulsion aircraft. However, these efforts do not take into account some key disciplines, such as thermal aspects and efficiencies.

Sgueglia et al. [32,33] presented a revised conceptual design process that overcomes these limitations: in particular, concerning

the thermal management and the trajectory simulation, as well as considering an aircraft featuring distributed electric propulsion. They considered all the key disciplines (aerodynamics, weights, structure, performance, thermal) for a large passenger aircraft with distributed electric propulsion. The level of detail achieved was still limited to the conceptual design level since they used low-fidelity models, such as semiempirical equations and the vortex-lattice method (VLM). Also, they considered modifications in the multidisciplinary design analysis (MDA) loop; but, as stated by Brelje and Martins [1], an MDA approach may neglect relevant coupled features in the design of unconventional configurations. They identified multidisciplinary design analysis and optimization (MDAO, also referred to as MDO) as the only way to deal with unconventional configurations [34]. MDO is a solution to deal with problems that present interactions between disciplines, due to its ability to take these interactions into account in reaching an optimal configuration [35], as demonstrated by Hwang and Ning [36].

Brelje and Martins [35] presented an open source framework that includes the optimization of small aircraft that considers mission trajectory. While this is a good step toward the optimization of hybrid-electric aircraft, it still relies on simplified assumptions, such as constant efficiency and specific fuel consumption over the trajectory. Most of the published work on hybrid-electric aircraft sizing has focused on the design of propeller-driven regional aircraft [30,37,38]; however, large transport aircraft represent a wide segment of commercial aviation.^{***} Thus, considering the integration of hybrid-electric propulsion for large transport aircraft is of interest for next generation aircraft. There have been a few efforts in this area, such as the NASA N3-X concept [39] and the ONERA DRAGON (Distributed fans Research Aircraft with electric Generators by ONERA) [6]. Therefore, there is a need for the development of a full MDO procedure for the design optimization of large transport hybrid aircraft [1].

This work extends the work of Sgueglia et al. [32], developing the procedure for the conceptual design of hybrid aircraft that use MDO. The main objective is to develop a tool for the design optimization and performance evaluation of hybrid-electric aircraft at the conceptual level, where all key disciplines are modeled with low fidelity to keep the computational cost low. The developed framework computes gradients for use with gradient-based optimization [34,35]. At this stage, the aircraft is evaluated by only considering its performance; stability, control, as well as operational aspects are not taken into account.

To fulfill this goal, the existing sizing tool FAST (which stands for fixed-wing aircraft sizing tool) [40] is implemented within the OpenMDAO framework [41,42]. FAST is an aircraft sizing tool that has already been tested on a large variety of configurations including turbojet [40,43,44], turboprop [45], and blended-wing–body aircraft [46,47].

OpenMDAO is an optimization framework that implements the MAUD (modular analysis and unified derivatives) architecture [42], which is an efficient way to compute coupled derivatives. Together with gradient-based optimization, this enables the solution of large-scale optimization problems [41]. OpenMDAO has been extensively used for various applications, such as aerostructural optimization [48], topology optimization [49], on-demand air mobility [36], small satellite design [50], aircraft design optimization with airline profit analysis [51], and BLI optimization using high-fidelity tools [22,52]. In this work, we use OpenMDAO version 2.4.^{†††}

This paper describes the development of this integrated hybrid-electric aircraft analysis and design optimization framework, and it presents the results of its application to the design of a large transport aircraft with distributed propulsion. Section II presents a brief overview of the aircraft concept, which has been detailed in previous work [32]. Section III presents the integration between FAST and OpenMDAO, which represents the core development of the present work. This required the redevelopment of the aircraft design framework FAST to use the OpenMDAO features. The resulting tool is then demonstrated by performing the design optimization of the hybrid-

^{***}Data available online at http://www.boeing.com/resources/boeingdotcom/commercial/about-our-market/assets/downloads/cmo_print_2016_final_updated.pdf [retrieved 08 June 2019].

^{†††}Data available online at <http://openmdao.org/twodocs/versions/2.4.0/index.html> [retrieved 08 June 2019].

[†]Collier, F., and Wahls, R., “ARMD Strategic Thrust 3: Ultra-Efficient Commercial Vehicles Subsonic Transport,” 2016, <https://www.nasa.gov/sites/default/files/atoms/files/armd-sip-thrust-3a-508.pdf>.

electric aircraft in Sec. IV. We compare the developed tool with the original version of FAST, citing both advantages and drawbacks. We also compare the resulting optimal designs. Finally, Sec. V summarizes the findings of our work.

II. Hybrid-Electric Aircraft Concept

A. Aircraft Modeling

The case study considered in this work is a hybrid-electric large passenger aircraft with distributed electric fans previously proposed and studied by Sgueglia et al. [32]. This aircraft concept, shown in Fig. 1, assumes an entry into service (EIS) in 2035. The main features of this concept are that it flies fully electric, at least up to 3000 ft (about 1 km), to reduce the emissions in the mean atmospheric boundary layer, where the convective effects are the most significant [53].

In this concept, the batteries are coupled with two turbogenerators (a combination of a gas turbine and an electric generator) that supply the power to the distributed ducted fans. Among all the possible choices for the position of the fans, the wing upper inner surface is chosen to increase the wing circulation [54]. This increases the maximum lift coefficient [10,11], making it possible to reduce the wing area, shorten the takeoff field length, or both. In addition, this concept is expected to save weight because of the absence of high-lift devices.

The main advantage of distributed propulsion is the potential to increase propulsive efficiency relative to conventional aircraft [7,17,55]. Due to the larger number of fans, it is possible to reduce the fan pressure ratio, leading to a propulsive efficiency larger than 0.9

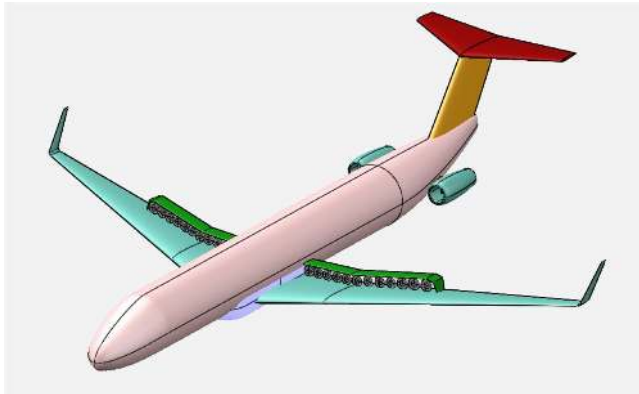


Fig. 1 Hybrid-aircraft concept with distributed electric ducted fan, proposed in Ref. [32].

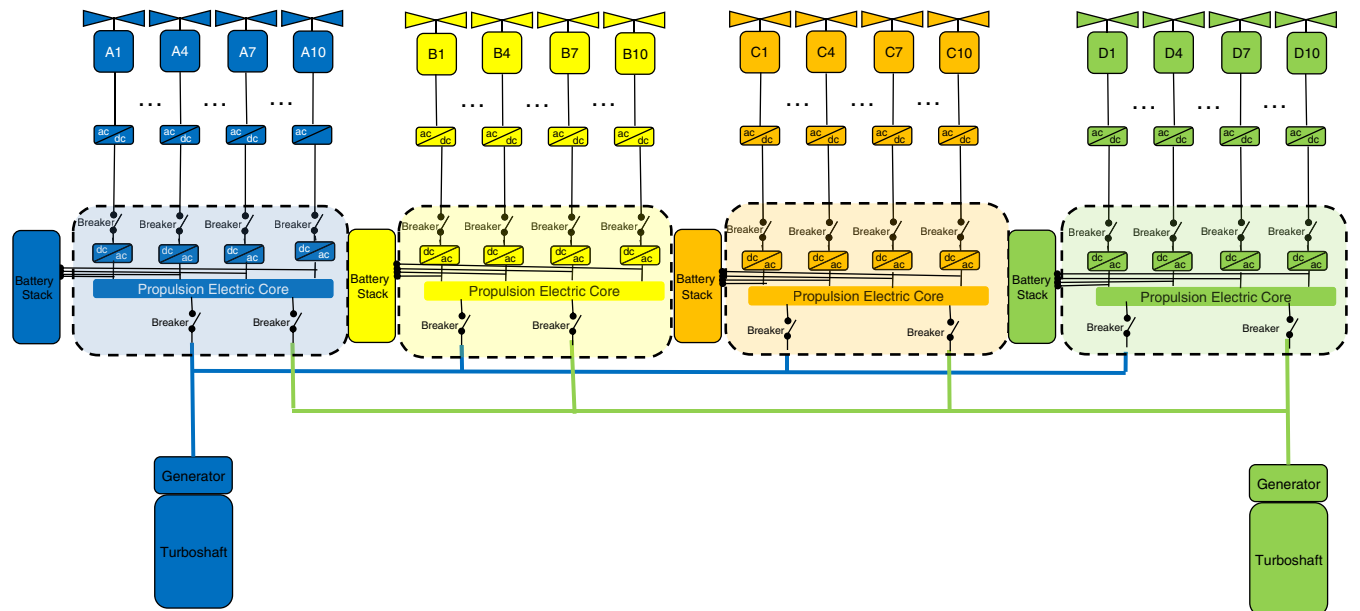


Fig. 2 Propulsive system architecture used in the proposed hybrid-electric concept, considering (as examples) 40 engines distributed along the wing.

[2]. Distributed propulsion also improves the aerodynamics [30,31], but this effect is of second order compared to the overwing blowing and can be neglected at the conceptual design level stage [56].

Turbogenerators are located at the rear to reduce the pylons' wetted area and avoid interference with the wing. Their position also increases passenger safety since they are far from the cabin. A T-tail is adopted because of the turbogenerators' location. Batteries are located in the cargo area, split between the regions ahead of and behind the wing. This choice is dictated by the available volume and center of gravity positioning; the battery weight is significant and is the component that affects the center of gravity the most. The aircraft center of gravity is located around the center of gravity of the wing; so, with this arrangement, the batteries do not move it significantly.

The fuselage weight is also affected by the batteries, due to the reinforcement to carry their weight. Preliminary studies show that the penalty is 5% for the baseline case. Linear extrapolation is considered for different values of battery volume. The percentage already includes a margin to be conservative. The maximum payload is decreased as well, since only part of the cargo area is available for luggage.

The core of the new concept is the hybrid-electric chain definition, which is described in the next section together with the description of most relevant models.

B. Propulsive System Architecture

The propulsive system is depicted in Fig. 2, considering 40 distributed electric motors. As described in the previous section, batteries and generators are coupled to supply electric power. These are connected through a set of electrical buses. An electric line connects each power source to all the buses to avoid power losses in case of a bus failure. From these devices, the lines provide power to the electric motors and the ducted fans. Inverters convert the current type from dc to ac, and vice versa. In the battery package, converters are used to bring current to the right transport voltage. Finally, breakers are installed to disconnect a line in case of failure.

The propulsion system architecture shows two different energy sources, and it intrinsically introduces a redundancy since, in case of failure of one energy source, the other can react to keep the required level of thrust. The propulsion system is sized by the case where one of the electric cores becomes inoperative. In this case, no loss of power is detected, but it must be distributed over a reduced number of components, resulting in an oversizing [56,57]. The propulsion system sizing is detailed in the next section.

When dealing with electric components, the key parameters are the specific energy and the specific power density, following the notation used by Brelje and Martins [1]. These quantities are represented as

Table 1 Summary of the methods implemented in FAST for each of the disciplines included in the conceptual design process

| Discipline | Method | Reference(s) |
|----------------|------------------------------|--------------|
| Geometry | Statistical equations | [59,61,62] |
| Aerodynamics | Semiempirical equations, VLM | [60,63] |
| Mass breakdown | Statistical equations | [64] |
| Performance | Time step approach | [65] |

subscripts e for specific energy density and p for specific power density. A detailed description of all the models adopted in this study can be found in previous work [32]. The electric components are sized by considering their power density and the maximum power demand, and the gas turbine is modeled with Gas turbine Simulation Program (GSP) [58]. We use a simplified model of the batteries that is detailed in the next section.

III. Aircraft Design Optimization Framework

A. Initial Sizing Loop for Hybrid-Electric Aircraft

As previously mentioned, we use the aircraft design tool FAST [40]. This is a multidisciplinary design analysis tool developed in Python and tailored for the conceptual design and performance evaluation for a given set of top-level aircraft requirements (TLARs). Inputs are given through an XML (eXtended Matrix Language) file, which works also as an output file and stores the results of the sizing. FAST has been validated for the CERAS (CEntral Reference Aircraft data System) reference aircraft,^{***} which is a public database that emulates the A320 aircraft. Results of this validation are detailed in Ref. [40].

FAST is a low-fidelity tool: aerodynamic and mass estimation methods come from statistical data and empirical equations contained in classical design handbooks [59,60]. Table 1 lists the methods implemented in FAST and provides the corresponding references [59–65].

Sgueglia et al. [32] developed a version of FAST tailored to the sizing of hybrid-electric aircraft, which we refer to as the *original version*. Algorithm 1 can be graphically represented using the XDSTM

Algorithm 1: FAST algorithm description, as used in the version presented in Ref. [32] for the sizing of a hybrid-electric aircraft (original version)

Require: Top-level aircraft requirements
Ensure: Sized aircraft, drag polars, masses, design mission trajectory

- 0: An initial guess for weight wing surface DEP components is computed using statistical methods from Raymer's book [60].
- repeat**
- 1: Initialize the loop.
- 2: Size the battery, according to power and energy requirements.
- 3: Size the wing, according to fuel and approach requirements.
- 4: Compute initial geometry, starting from a set of geometrical inputs.
- 5: Resize the geometry and locate center of gravity. At each iteration, mass estimation is carried out to evaluate the center of gravity position.
- 6: Aerodynamic calculation, based on sem-empirical equations and VLM.
- 7: Mass breakdown calculation, with the final values coming from analysis 5.
- 8: Evaluate performance.
- 9: Update maximum takeoff weight (MTOW), considering the difference in operating empty weight (OEW) coming from mass calculation (step 7) and performance (step 8).
- 10: Check convergence criteria: if they are satisfied, it ends the loop; otherwise it proceeds to next iteration.

until 10 → 2: MDA has converged

standard [66]. In this notation, the purple circular block represents the optimizer; meanwhile, the orange one refers to an MDA loop. Green blocks represent the analysis, and they are numbered according to the order of processing; and pink rectangles represent the functions.

Figure 3 depicts the FAST sizing loop in this standard. The main workflow is identified by the black line, whereas gray lines denote/identify/represent the data sharing between analyses. Analysis outputs are indicated with a gray block; finally, I/O data are identified with a white block: inputs are at the top row, and outputs are at the left column. The notation x represents the design variables vector, y are the state variables, apex (0) indicates an initial guess, t is a target variable (that is, a variable that is a copy of a previous output), and $*$ is the final value.

The driven parameter for the procedure is the operating empty weight: its value is estimated at step 7, after the mass breakdown (OEW_{mb}), and at step 8, after the performance calculation, as OEW_{perfo} = MTOW – m_f – PL. At convergence, these two values must match; if not, the MTOW is updated for next iteration as in Eq. (1):

$$\text{MTOW}_{i+1} = \text{MTOW}_i + (\text{OEW}_{\text{mb}} - \text{OEW}_{\text{perfo}}) \quad (1)$$

In practice, the tolerance for convergence is set to 10^{-3} ; that is, the relative difference between the two values of OEW must not exceed 0.1%.

Compared to a classical design loop, in the reviewed procedure, there is a new analysis called “battery sizing” (step 2 in the preceding algorithm) to properly size the battery according to the energy and power requirements. Then, other changes are present at steps 4 and 5 to consider the presence of batteries, the ducted fan, and generators; and then in step 8, to consider the double energy source in the performance calculation. In the next sections, the essential notions of modeling adopted for geometry, mass estimation, performance, and certification are provided.

1. Geometry

The geometry module is devoted to the estimation of the aircraft dimensions, as well as the center of gravity placement. The aircraft geometry is decomposed in five elements: fuselage, wing, horizontal and vertical tails, and nacelle. Each of these elements needs a set of variables to be fully defined.

The fuselage only needs the number of passengers and the seat's dimensions to estimate the width and the total length, according to the methods provided by Roskam [62].

As seen also from Algorithm 1, the wing area is estimated out of the geometry module at step 2; wing dimensions are computed together with other dimensions in step 3. The wing area is estimated by considering two criteria: approach condition and fuel stored. The first condition is represented by Eq. (2), where MLW is the maximum landing weight, V_s is the stall speed given in the TLAR, $C_{L_{\text{max}}}$ is the maximum lift coefficient in the landing configuration, and $S_{w_{\text{app}}}$ is the value of wing area that satisfies the equation:

$$\text{MLW}g = \frac{1}{2}\rho V_s^2 S_{w_{\text{app}}} C_{L_{\text{max}}} \quad (2)$$

The second condition is more complicated. The maximum fuel weight (MFW) that can be stored in the wing can be expressed as

$$\text{MFW} = f\left(S_{w_f}, AR_w, \left(\frac{t}{c}\right)_w\right) = k_1 S_{w_f}^{1.5} AR_w^{-0.4} \left(\frac{t}{c}\right)_w + k_2 \quad (3)$$

where S_{w_f} is a value of the surface, AR_w is the wing aspect ratio, $(t/c)_w$ is the mean thickness-to-chord ratio, and k_1 and k_2 are constant parameters that depend on the type of aircraft. Imposing $m_f = \text{MFW}$, with m_f being the fuel needed for the design mission, yields an estimation of the wing area that satisfies the condition. Finally, the value of the wing area is the maximum of $S_{w_{\text{app}}}$ and S_{w_f} .

Once the wing area is known, the planform can be obtained. The parametrization adopted is shown in Fig. 4: the wing geometry is a two-section wing, with the break located at station y_k . Assuming that the break is at 40% of the semispan and that the trailing edge has an angle equal to zero in the inner section, the wing planform is then defined by four parameters: wing area; wing aspect ratio AR_w ; wing sweep angle, evaluated at 25% of the chord $\Lambda_{25\%}$; and the taper ratio $\lambda_w = c_i/c_r$. In addition, the thickness-to-chord ratio is needed for aerodynamic evaluations.

^{***}Data available online at <https://ceras.ilr.rwth-aachen.de/>.

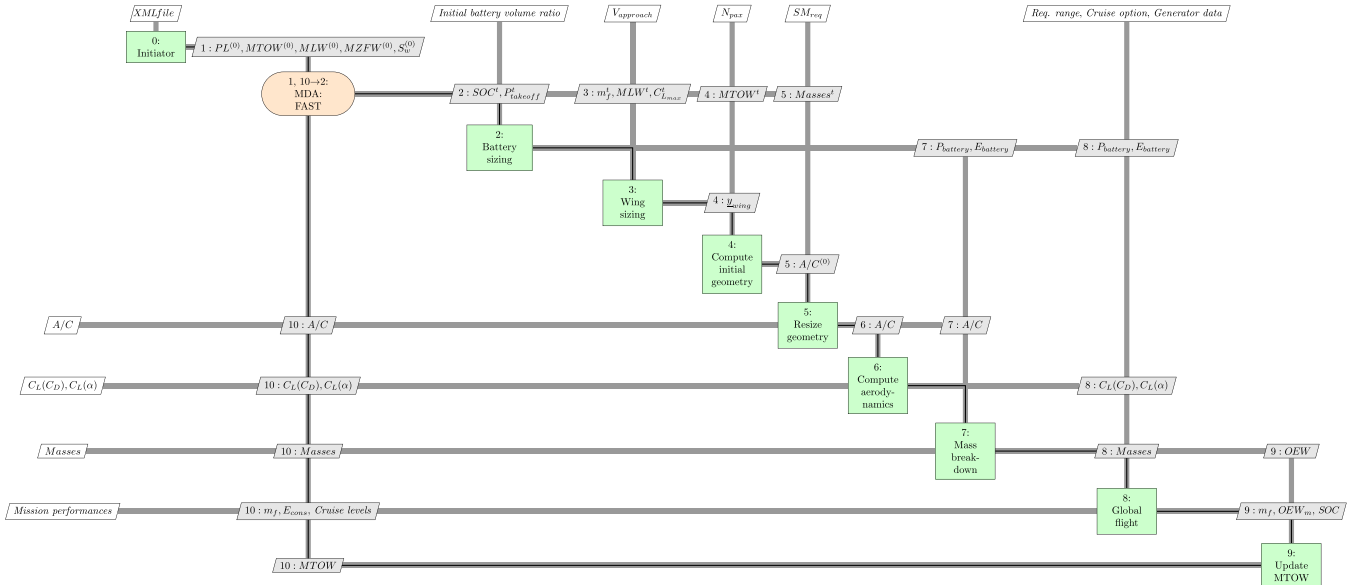


Fig. 3 Original version FAST XDSM, as used in Ref. [32]. Figure refers to Algorithm 1. (A/C = aircraft, CG = center of gravity, Req = required.)

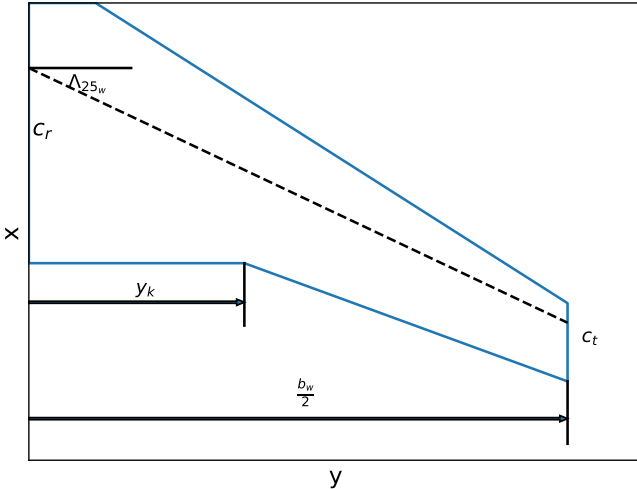


Fig. 4 Wing parametrization used in geometry module for FAST; only half-wing is shown because of symmetry. It consists of a two-section wing, with the break placed at the station y_k ; chord distribution is obtained from the knowledge of the sweep angle at 25% of the chord Λ_{25_w} .

Horizontal and vertical tail geometries show a similar procedure, with the difference that they have just a single section in place of two.

Fan dimensions are obtained by the knowledge of the fan pressure ratio (FPR) and the design thrust, with the procedure explained in the work of Sgueglia et al. [32]. From the knowledge of the fan radius r_f , the length of the nacelle is obtained as $1.05 \times 2N_{EM}r_f$, where the factor of 1.05 accounts for some space margin between fans and the nacelle.

At this point, the first limitation of the code comes out: in case the fans do not fit in the available space on the wing, an error message appears, but no actions are automatically taken by the code. It is up to users to modify inputs in order to have a feasible solution.

Finally, the battery volume is computed in the geometry module too. Their sizing recalls the wing area sizing: they need to satisfy two criteria and, at the end, the maximum volume between the two values is taken. In particular, the conditions are related to energy and power requirements. The first one ensures that batteries can store all the energy available, with a 20% safety margin [67,68], and can be expressed through the definition of the State Of Charge (SOC):

$$\text{SoC}(t_f) = 1 - \frac{E_c(t_f)}{E_b} \geq 0.20 \quad (4)$$

where E_c is the energy consumption, E_b is the battery energy stored, and t_f indicates the final mission time. In reality, the SOC is defined using the capacity notion (current multiplied by the time step) [67]; however, the assumption of constant voltage leads to Eq. (4).

The second condition ensures, instead, that batteries can deliver all the power required for a required phase of flight P_{ref} :

$$N_b P_b \geq P_{\text{ref}} \quad (5)$$

where N_b and P_b indicate the number of batteries and the maximum power delivered by each battery, respectively. Imposing the equality in Eqs. (4) and (5) yields an estimation of the minimum volume needed to satisfy each condition; the maximum between the two is the actual value of battery volume. The reference power may be the power required during any phase of flight (takeoff, climb, ...); the condition will be further detailed in one of the next paragraphs.

2. Mass Estimation

For the mass and the center of gravity estimation, a breakdown standard must be chosen. This choice is arbitrary and left to designers; in FAST, the standard follows the rules of reference French norm 2001/D [40,64]. Models for mass estimation of the components rely on semiempirical methods; the standard is limited to the conventional aircraft, and the mass associated to the hybrid-electric powerplant must be added. Following the example of some authors [16,69–72], mass is estimated by the knowledge of the power-to-mass ratio as

$$m_i = \frac{P_{\text{max}_i}}{p_i} \quad (6)$$

where the subscript i indicates a generic electric component, and P_{max_i} is the maximum power demanded.

3. Aerodynamics

The aerodynamic model computes the drag polar, in low and high speeds. The drag coefficient is decomposed into four terms:

$$C_D = C_{D_0} + C_{D_i} + C_{D_w} + C_{D_{\text{eq}}} \quad (7)$$

where C_{D_0} represents the term related to friction, C_{D_i} is the induced drag, C_{D_w} is the wave drag for the transonic regime, and $C_{D_{\text{eq}}}$ is a term related to trim condition.

All these terms are obtained using the methods provided by Roskam [63]. To compute the C_{D_0} , friction coefficient for each

subcomponent (wing, fuselage and tails) is estimated based on their wetted surface, then the global value is obtained as a weighted mean value among these coefficients. Effects related to thickness are modeled through linear corrective factors.

For the induced drag, it is assumed that only the wing produces lift; in other words, the contribution of the horizontal tail is neglected, as suggested by some authors [73]. The term C_{D_i} is then computed using its classical formulation coming from the Prandtl theory [74]:

$$C_{D_i} = \frac{C_L^2}{\pi A R_w k_e} \quad (8)$$

where C_L is the lift coefficient, and k_e is the Oswald factor, estimated using the method proposed by Niřa and Scholz [75]. The other two terms, related to wave drag and trim, are estimated by considering linear dependency with geometric parameters like sweep and thickness.

No modifications due to hybrid propulsion are considered for the polars, other than estimating the parasite drag of the nacelle using the method described earlier in this paper.

At low speed, a value of $C_{L_{max}} = 4.5$ is considered to model the blowing phenomenon [11,56,57]. The following assumptions are made:

- 1) Blowing is relevant only at low speed and maximum thrust: that is, at takeoff. Its effects in cruise are neglected.
- 2) The only effect is on the value of $C_{L_{max}}$; the impact on the slope C_{L_α} is neglected [56].

4. Performance Evaluation

Performance is evaluated through the computation of the mission profile using a time-integration approach. The mission profile is made up of takeoff, initial climb, climb, cruise, descent, and an alternate flight plus a holding phase for reserve. The trajectory is obtained by solving the flight equations with the time-marching approach for each phase. It is also assumed that the cruise starts at the point of maximum lift-to-drag ratio, and then the aircraft climbs gradually to fly always at $C_L = C_{L_{opt}}$ (cruise climb approach). To find the right initial cruise point, an iterative loop is needed: cruise altitude is changed and the climb phase iterated until the condition $C_L = C_{L_{opt}}$ is met.

Since this is a hybrid-electric concept, at each time step, both the fuel and the energy consumption are evaluated. Knowing the actual state of the aircraft at step i (that is, its C_L and C_D), it is possible to

obtain the power required by batteries and turboshaft (P_{b_i} and P_{ts_i} , respectively) to sustain the flight and the value of power specific fuel consumption (PSFC) of turboshaft engines. The values of fuel and energy consumption are then updated using

$$m_{f_{i+1}} = m_{f_i} + N_{ts} P_{ts_i} \text{PSFC}_i \Delta t \quad (9)$$

$$E_{c_{i+1}} = E_{c_i} + N_b P_{b_i} \Delta t \quad (10)$$

where Δt is the time step. Using Eq. (4) for the time step i , the SOC is updated as well; finally, the mass of the aircraft at time step $i + 1$ is obtained by subtracting the fuel consumed during the time step i . This procedure is iterated for each segment until termination.

During the cruise step, the code calls the function for descent phase at the end of each time step to check if the total distance covered is equal to the range. If this is not the case, the process moves to next time step. The procedure is depicted in Fig. 5 using the XDSM standard. The scheme highlights the iterative loops implemented: from steps 0 to 2, the climb is iteratively called until the cruise altitude is obtained to match the condition of optimal flight point. Then, steps 3–7 implement the time step approach: for each time step, the code obtains the distance travelled in cruise thus far (step 4), and then it performs the descent (step 5). Afterward, step 6 takes as an input the distance travelled during climb, cruise, and descent, and checks if it is equal to the design range; if not, it proceeds to the next time step.

The implementation is very costly since it requires a call to the descent function thousands of times for a single sizing iteration, which is a limitation of the code used here.

5. Certification Constraint Module

Finally, once that trajectory is obtained, an analysis on certification is carried out through the certification constraint module (CCM) [43]. This module checks if the specifications given by CS-25 [76] are satisfied. In addition, the EASA acceptable means of compliant Part CAT document [77] for operational requirements is also considered: although it is not related to certifications, it is of great importance to have an aircraft satisfy these specifications. Conditions implemented in the code are listed as follows:

- 1) Reserve of vertical speed at top of climb and top of descent of at least 300 ft/min, as prescribed by CAT.POL.A.410(a)-1 and 2 [77].
- 2) Steady gradient flight, in landing configuration and with all engines operative (AEO condition) of at least 3.2%, as prescribed by CS-25.119(a) [76].

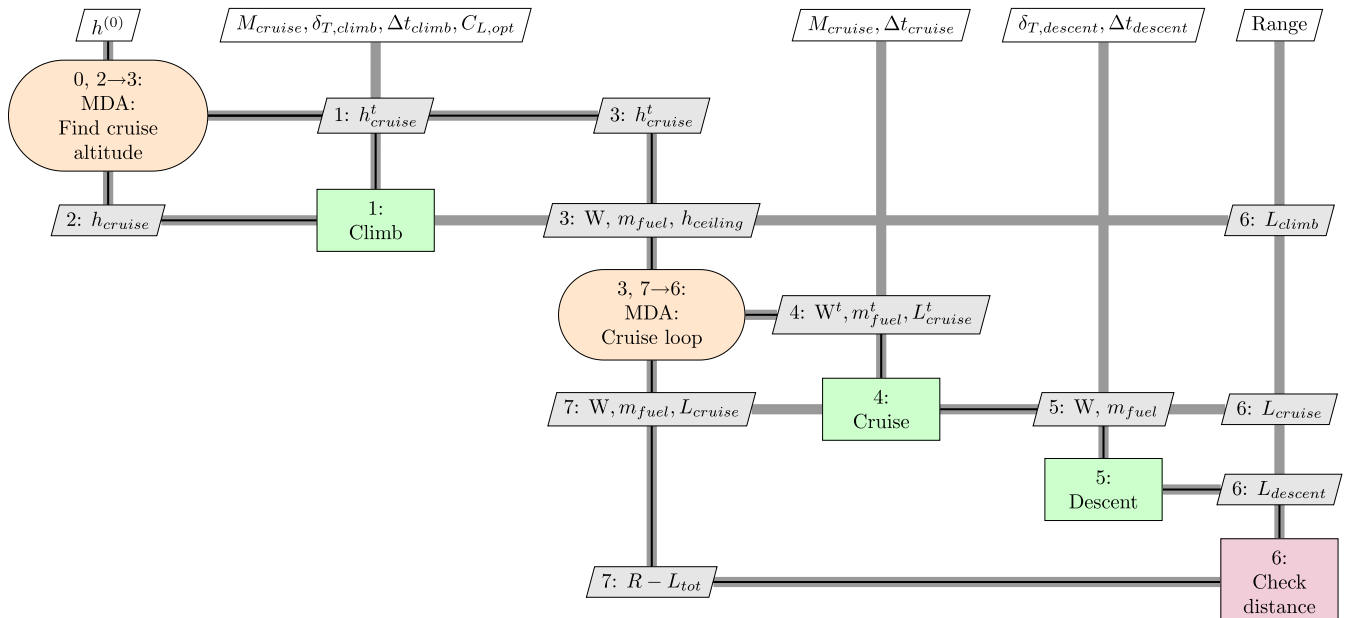


Fig. 5 Scheme of the performance module in FAST using the XDSM standard, limited to the climb, cruise, and descent. The scheme highlights the time step approach, which is implemented in FAST.

3) Steady gradient flight, in takeoff configuration and with one engine operative (OEI condition) greater than zero, as prescribed by CS-25.121(a) [76].

4) Steady gradient flight, in takeoff configuration at 400 ft of altitude and in OEI condition of at least 2.4%, as prescribed by CS-25.121(b) [76].

5) Steady gradient flight, at the end of takeoff phase and in OEI condition of at least 1.2%, as prescribed by CS-25.121(c) [76].

6) Steady gradient flight, in approach configuration and AEO condition of at least 2.1%, as prescribed by CS-25.121(d) [76].

In the case of distributed propulsion, the OEI condition is meaningless since a loss of one engine is not relevant as for conventional aircraft [57,78,79]. Also, given the two energy sources, the failure case is not clear. Two different situations may occur: failure of an energy source, which leads to a loss in total thrust available; and failure of an electric core, which leads to a set of electric motors becoming inoperative (see Fig. 2). In this work, the first condition is not considered since it is assumed that in, case one source becomes inoperative, the second can always provide supplementary power to avoid loss of total thrust.

The second condition, hereby called one core inoperative (OCI), instead represents the sizing case for electric components since there is no loss of total power, but it has to be distributed over a reduced number of electric components. This situation leads to an oversizing of electric components, and it has been considered as a failure case. Table 2 reports the proposed certification rules for the hybrid-electric concept studied here. This table highlights that the CCM only checks if the constraints are satisfied; if they are not, it is up to users to manually edit some TLARs or input in order to comply with specifications.

Regarding the pending question of the reference power for battery and other electric components sizing, it should be the minimum power that guarantees all the specifications of Table 2 are satisfied. Unfortunately, this is not known a priori and, since the CCM performs only a check, is not possible to get this power from the application.

Some trade studies [57] show that the most stringent condition is the CS-25.121(b) [76], which requires the gradient flight at 400 ft, in the OCI condition, must be greater than 2.4%: this condition is retained for the sizing.

So far, the code presented in previous paragraphs is tailored only for sizing; its integration within an optimization framework is the goal of the next section.

B. Optimization Algorithm for Hybrid-Electric Aircraft

To enable optimization with the FAST models, it is integrated with OpenMDAO 2.4 [41] to address design challenges of the unconventional concept proposed here. The main OpenMDAO building blocks are the `Components`, which map inputs to outputs in either an implicit or explicit formulation. `Components` represent the starting point from which complex models are built up. They may represent a discipline in simpler models but, most of the time, they represent only a small part of a discipline (e.g., for aerodynamics, each component may represent a single contribution to the drag coefficient). An ensemble of different `Components` is called a `Group`, which is a higher level of OpenMDAO hierarchy. A discipline is typically represented by a `Group`. To give a practical example, in the case

of the aerodynamics module, `Components` may be defined to compute a single contribution to the drag polar; their regrouping to get the total drag coefficient occurs in a `Group`, which represents the aerodynamic discipline. This logic allows one to have flexibility since it is always possible to easily add or remove analysis from a problem.

To perform the integration between FAST and OpenMDAO, the original code was modified by decomposing each module in a set of `Components`, and then it was regrouped to form disciplines (geometry, mass breakdown, aerodynamic, and performance). To differentiate from the original version, the developed framework is hereafter referred to as the “integrated version.”

Because of the choice to define the MDO based on analytic derivatives, each `Component` computes no more than three equations at a time to simplify the derivation of analytic derivatives. In OpenMDAO, the total derivatives are obtained from the knowledge of partial derivatives for all components; therefore, for each component’s output, its derivatives with respect to inputs must be analytically defined.

Algorithm 2 presents the new optimization procedure; the corresponding XDSM scheme is shown in Fig. 6. The green blocks here

Algorithm 2: Updated FAST algorithm description, tailored to perform an optimization of a hybrid-electric concept (integrated version).

Require: Initial design parameters (TLARs), design variables initial vector $\mathbf{x}^{(0)}$.

Ensure: Sized aircraft, drag polars, masses, performances/

0: Initialize the optimization loop: the starting point $\mathbf{x}^{(0)}$ is read from the XML file.

repeat

1: Compute the battery parameters (power and energy stored).

2: Initialize the MDA, used to get a feasible aircraft.

repeat

3: Update the MTOW at each iteration, according to values of OEW coming from previous iteration.

4: Compute the aircraft geometry, by the knowledge of the design vector \mathbf{x} and other top-level input parameters, and perform the mass breakdown to estimate weight of all components.

5: Compute the static margin. C_L slope for wing and horizontal are estimated from the geometry defined in previous analysis.

6: Aerodynamic calculation, based on the same equations of the original version, described in Sec. III.A.3.

7: Compute the aircraft performance.

8: Convergence check. The control parameter to ensure the convergence is the OEW; the criterion is the same as of the original version of the code.

until 8 \rightarrow 3: MDA has converged

9: Evaluate the objective function.

10: Evaluate the design constraints.

11: Check if the optimization has converged. If not, \mathbf{x} is updated for the next iteration.

until 11 \rightarrow 1: MDO has converged and the final design variables vector \mathbf{x}^* is found.

represent a single discipline, as in the scheme of Fig. 3, but each block is not a `Component` but rather a `Group`.

The resulting MDO architecture is called multidisciplinary feasible (MDF) [34]: in this kind of architecture, the optimizer directly controls \mathbf{x} , $f(\mathbf{x})$, and $\mathbf{g}(\mathbf{x})$. The main MDF benefit is that, in case the optimization terminates earlier, the resulting system design is always feasible, which is a key point for designers since it is possible to establish a tradeoff even in case of nonconverged simulations (that is, the solution may not be optimal in a mathematical sense) [34]. The main disadvantage, instead, is that it requires a full MDA to be performed at every optimization iteration: in the integrated version, steps 3–8 in Algorithm 2 represent the sizing process, that is, the MDA. In addition, total derivatives of the full MDA are required.

The integrated version has been run once, without optimization, starting from the configuration studied in Ref. [32] to ensure the result is the same and no error occurred during the development. The validation results, considering $N_{EM} = 40$ and $R = 1200$ n miles,

Table 2 CS-25 [76] and CATPOL [77] rules revised for the hybrid-electric concept^a

| Certification | Phase | Condition | Parameter | Minimum value |
|--------------------|----------------|-----------|------------|---------------|
| CAT.POL.A.410(a)-1 | Top of climb | AEO | V_z | 300 ft/min |
| CAT.POL.A.410(a)-2 | Top of descent | AEO | V_z | 300 ft/min |
| CS-25.119(a) | Landing | AEO | $\gamma\%$ | 3.2% |
| CS-25.121(a) | Takeoff | OCI | $\gamma\%$ | 0% |
| CS-25.121(b) | 400 ft | OCI | $\gamma\%$ | 2.4% |
| CS-25.121(c) | End of takeoff | OCI | $\gamma\%$ | 1.2% |
| CS-25.121(d) | Approach | AEO | $\gamma\%$ | 2.1% |

^a V_z represents vertical speed; meanwhile, $\gamma\%$ is the gradient flight given in percentage.

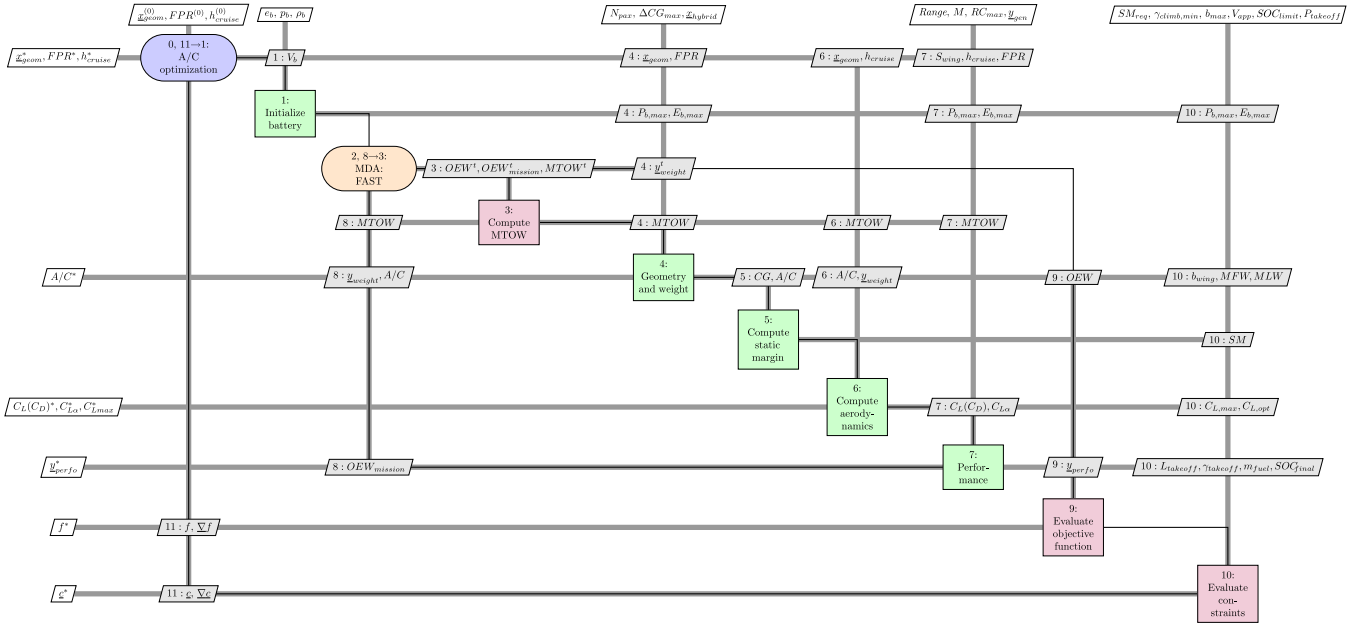


Fig. 6 Integrated version FAST XDSM, tuned for optimization of hybrid-electric aircraft. The MDO is detailed in Algorithm 2. (RC = rate of climb.)

are reported in Table 3. The difference is below 0.5% and can be considered negligible.

The original and the integrated versions present differences in the way the overall aircraft design problem is coded and solved; they are listed in the following:

1) The original version shows only one MDA loop, whereas in the integrated version, two loops appear: the outer one is the optimization loop; meanwhile, the inner one is the MDA, which is used to get a viable aircraft.

2) In the integrated version, design constraints are used in place of sizing criteria. This means that step 2 of Algorithm 1 is removed since the wing area parameter belongs to design variables. Equations (2) and (3) are rewritten as design constraints; the solver lets S_w vary in its design space and, at convergence, it automatically finds the optimal value that satisfies design constraints. The same approach applies to battery, tail sizing, cruise altitude matching and center of gravity assessment. At each optimization iteration, the code only needs to compute the geometry once and check the stability conditions; if design constraints are not satisfied, the optimization solver finds a new value of wing position.

3) A consequence of the previous point is one of the peculiarities of the new integrated formulation: in this approach, it is not the case that each optimization iteration produces an aircraft that satisfies all the design constraints; whereas in the original code, at the end of each iteration, a feasible aircraft (in terms of wing, tail sizing criteria, and stability) was obtained.

4) In the original version, the starting point was initialized before the loop using statistical equations; in the integrated version, instead, it is randomly chosen within the design space.

5) The iterative routine available in OpenMDAO makes the code more efficient. The main example of this is in the performance calculation: as highlighted in Sec. III.A.4, at each cruise point, it carries out the descent to check the distance covered, which results in an expensive procedure. In the integrated version, instead, the OpenMDAO routines

just need the distance to travel in cruise; then, they iteratively change this value to cover the total range considering climb and descent lengths.

All the differences listed previously make the integrated version more efficiently coded: the absence of iterative loops in the geometry and, overall, in the performance module reduce the computational cost by a factor of five for the validation case reported in Table 3.

In the original version, a fixed point iteration was used for every loop. OpenMDAO, instead, presents a large variety of numerical schemes that can be used to solve iterative loops. This affects the robustness since a choice of proper scheme may accelerate the convergence or allow for a more accurate result: in fact, the MDA tolerance is reduced by three orders of magnitude, from 10^{-3} to 10^{-6} .

Despite these advantages, the integrated version presents some drawbacks: in the integrated version, there are more than 200 OpenMDAO Components associated with the discipline to facilitate analytic gradient computation compared to the 19 of the original one. This can make it hard for a new user to understand how to modify the code.

At this stage, the MDO procedure is set. The next section reports the associated optimization problem.

C. Problem Definition

An optimization problem is mathematically defined as

$$\begin{cases} \text{minimize} & f(\mathbf{x}) \\ \text{with respect to} & \mathbf{x} \in \mathbb{R}^n \\ \text{subject to} & \mathbf{c}(\mathbf{x}) \in \mathbb{R}^d \end{cases}$$

where $f(\mathbf{x})$ is the objective function, \mathbf{x} is the design variables vector, $\mathbf{c}(\mathbf{x})$ is the constraint vector, n is the problem size, and d is the constraint size. All these elements must be defined; Table 4 sums up this definition. The optimization problem consists of 20 design variables, subject to a total of 17 design constraints. The bounds of variables are chosen by considering a large number of existing aircraft of the same category [61].

The objective function $f(\mathbf{x})$ can be fuel, energy consumption, or even more complex functions. The design vector \mathbf{x} contains geometrical (for wing and tails), propulsive, and mission variables. Note that they must be continuous, as OpenMDAO does not consider discrete variables in the optimization problem [41,80]. The choice of these parameters relies on the models adopted in FAST, following the parametrization shown in Fig. 4 and the comments reported in Sec. III.A. Battery volume τ_b is needed to properly size batteries.

Table 3 Results of validation between the original and the integrated version for the case presented in Ref. [32]: $N_{EM} = 40$ and $R = 1200$ n miles

| | Original | Integrated |
|------------------------|----------|------------|
| MTOW, t | 80.1 | 80.1 |
| OEW, t | 59.5 | 59.4 |
| Wing area, m^2 | 118.77 | 118.51 |
| Energy consumption, GJ | 305.61 | 305.68 |

Table 4 Optimization problem definition^{a,b,c}

| Category | Name | Size | Lower | Upper | Equals | Units | |
|-----------------|-------------------------------|--------|--------|-------|----------------|----------------|-----|
| Objective | $f(x)$ | 1 | --- | --- | --- | --- | |
| Variables | S_w | 1 | 100 | 150 | --- | m ² | |
| | x_w | 1 | 18 | 24 | --- | m | |
| | AR_w | 1 | 8 | 12 | --- | --- | |
| | λ_w | 1 | 0.2 | 0.6 | --- | --- | |
| | Λ_{25_w} | 1 | 20 | 45 | --- | deg | |
| | $(t/c)_w$ | 1 | 0.1 | 0.15 | --- | --- | |
| | S_{HT} | 1 | 20 | 80 | --- | m ² | |
| | AR_{HT} | 1 | 2 | 5 | --- | --- | |
| | λ_{HT} | 1 | 0.2 | 0.6 | --- | --- | |
| | $\Lambda_{25_{HT}}$ | 1 | 20 | 45 | --- | deg | |
| | $(t/c)_{HT}$ | 1 | 0.1 | 0.15 | --- | --- | |
| | S_{VT} | 1 | 15 | 50 | --- | m ² | |
| | AR_{VT} | 1 | 1 | 2.5 | --- | --- | |
| | λ_{VT} | 1 | 0.85 | 1.0 | --- | --- | |
| | $\Lambda_{25_{VT}}$ | 1 | 25 | 55 | --- | deg | |
| | $(t/c)_{VT}$ | 1 | 0.13 | 0.18 | --- | --- | |
| | P_{ref} | 1 | 6 | 15 | --- | MW | |
| τ_b | 1 | 1 | 3 | --- | m ³ | | |
| FPR | 1 | 1.05 | 1.4 | --- | --- | | |
| h_{toc} | 1 | 30,000 | 40,000 | --- | ft | | |
| Total variables | --- | 20 | --- | --- | --- | --- | |
| Constraints | Δm_f | 1 | 0 | --- | --- | kg | |
| | $\Delta C_{L_{app}}$ | 1 | 0 | --- | --- | --- | |
| | b_w | 1 | --- | 36 | --- | m | |
| | $\mathcal{M}_{takeoff}$ | 1 | --- | 0 | --- | N/m | |
| | $\Delta \mathcal{N}_{cruise}$ | 1 | 0 | --- | --- | N/m | |
| | SoC _f | 1 | --- | --- | 0.20 | --- | |
| | ΔP_b | 1 | 0 | --- | --- | W | |
| | Δl_{nac} | 1 | --- | 0 | --- | m | |
| | \bar{r}_f | 1 | --- | 0.15 | --- | --- | |
| | TOFL | 1 | --- | 2200 | --- | m | |
| | $\Delta C_{L_{toc}}$ | 1 | --- | --- | 0 | --- | |
| | SM | 1 | 0.05 | 0.10 | --- | --- | |
| | c_{CCM} | 5 | 0 | --- | --- | % | |
| | Total constraints | --- | 17 | --- | --- | --- | --- |

^aVariables are described by their bound constraint and their unit.

^bBounds come from data on a large number of tube-and-wing aircraft provided in Roskam's book [61].

^cInequality and equality constraints are also defined.

The propulsive design variables are the FPR (to control the power demanded by fan) and the sizing power for electric components P_{ref} (that must comply with certification aspects listed in Table 2). Cruise altitude h_{toc} is also needed to have continuity between segments. It is worth noting that none of the design variables are related to the turbogenerator; instead, this component is modeled outside the sizing loop because no sizing mode is available. Power and power specific fuel consumption curves are provided to FAST and interpolated to get the values of interest during the performance calculation.

The design constraints are described in the following:

1) The wing has to carry all the fuel needed and match the approach condition; these two criteria can be expressed as $\Delta m_f = MFW - m_f \geq 0$ and $\Delta C_{L_{ldg}} = C_{L_{max}} - C_{L_{app}} \geq 0$, respectively.

2) The horizontal tail and wing position are sized for two considerations: obtain rotational performances at takeoff and ensure that the static margin (SM) is between 5 and 10%. The first consideration requires that the longitudinal momentum balance is larger than zero (zero at limit) for a given maximum center of gravity variation ($\mathcal{M}_{takeoff} \geq 0$); meanwhile, the second consideration is simply quantified as $0.05 \leq SM \leq 0.10$. Note that this is a limitation since more aspects related to controllability play a role in the horizontal tail (HT) sizing and, due to the blowing, the effect is even more relevant in the

present case. However, as previously stated, this work only focuses on the performance evaluation and does not consider these aspects.

3) The vertical tail is sized to have lateral stability in cruise: S_{VT} has to ensure that the fuselage yaw moment is counterbalanced by the vertical tail yaw moment or in mathematical symbols $\Delta \mathcal{N}_{cruise} \geq 0$, with \mathcal{N} being the yaw moment.

4) The possibility to collocate all the engines in the available space is ensured by constraining the length of the nacelle: $\Delta l_{nac} \leq b_w - w_f$, with w_f being the fuselage width, which is not usable for fan allocations.

5) The fan must not be too big, to avoid structural problems. Defining a proper maximum dimension for the fan size is challenging; using the work of Wick et al. [54], a rough estimation of the allowable fan radius-to-chord ratio $\bar{r}_f = r_f/\bar{c}$, with \bar{c} being the mean aerodynamic chord (MAC), can be drawn. A reasonable threshold for this parameter is 0.15: that is, the fan radius must not exceed 15% of the MAC: this is expressed by $\bar{r}_f \leq 0.15$.

6) The wing span b_w and takeoff field length (TOFL) are limited by operational constraints for a medium range aircraft [81].^{§§§}

7) The state of charge at the end of the mission is fixed to 0.20 through an equality constraint to consume all the possible electrical energy, reducing fuel consumption.

8) The lift coefficient at the top of climb must be equal to the value that maximizes the lift-to-drag ratio to fly at the best altitude; in other words, $\Delta C_{L_{toc}} = C_{L_{toc}} - C_{L_{opt}} = 0$.

9) The certifications constraints may be expressed by defining a single vector

$$c_{CCM} = [V_{z_{toc}} - 300, V_{z_{tod}} - 300, \gamma_{\%_{119a}} - 3.2, \gamma_{\%_{121a}} \cdot \gamma_{\%_{121b}} - 2.4, \gamma_{\%_{121c}} - 1.2, \gamma_{\%_{121d}} - 2.1]$$

and imposing $c_{CCM} \geq 0$. To satisfy these conditions, P_{ref} is varied, but the wing area may also be impacted.

The next section will present the application of the integrated version of FAST on some test cases for the hybrid-electric aircraft featuring distributed propulsion.

IV. Optimization Results

This section presents the application of the new integrated version for the case study considered here. Results are divided as follows. At first, the top-level requirements are reported together with the technological assumptions reflecting an EIS of 2035. The following sections present the single-objective optimizations to assess the performance of the optimized architecture with respect to the conventional baseline in terms of fuel and energy consumption. Ultimately, a Pareto front is obtained, considering OEW and energy consumption, and using a gradient-free and a gradient-based method, in order to compare the two methods and show the gain using derivative information.

A. Top-Level Requirements for the Hybrid-Electric Aircraft

Table 5 reports the TLARs: they correspond to an A320-type aircraft (150 passengers). Range is not fixed yet because one of the main outcomes of Ref. [32] is that the zone of interest for design is limited to a range called breakdown range. This particular range represents the starting point after which the hybrid-electric aircraft is not advantageous anymore, and thus it is interesting to study performances varying this input.

As said in the previous section, discrete variables cannot be easily included in the optimization problem [80], and so the number of engines, batteries, and turbogenerators cannot be included in the optimization problem, but they are rather top-level entries. To understand the impact of this variable on the design, three different baselines varying N_{EM} from 16 to 48 are considered. The hybrid-electric concept is compared to a conventional aircraft, corresponding to a revised CERAS aircraft (see footnote ¶¶) resized to match the TLARs of Table 5 and optimized.

^{§§§}The ICAO Aerodrome Reference Code, International Civil Aviation Organisation, 2017, https://www.skybrary.aero/index.php/ICAO_Aerodrome_Reference_Code [retrieved 09 May 2020].

Table 5 Top-level aircraft requirements used to size the case study^a

| Parameter | Value | Unit |
|---|----------|---------|
| Range | 600–1500 | n miles |
| Mach number | 0.78 | — |
| Number of passengers | 150 | — |
| Design payload | 13,608 | kg |
| Number of electric motors | 16–48 | — |
| CAS (calibrated air speed) approach speed | 132 | kn |
| Maximum wing span | 36 | m |
| Maximum TOFL | 2.2 | km |

^aRange and number of engines are not fixed yet.

Table 6 Technological parameters for hybrid-electric chain components in the 2035 perspectives [32]

| Variable | Value | Unit |
|--------------|-------|----------|
| e_b | 500 | W · h/kg |
| $\rho_{E,b}$ | 850 | W · h/L |
| p_b | 2 | kW/kg |
| η_b | 0.9 | — |
| p_{EM} | 10 | kW/kg |
| η_{EM} | 0.98 | — |
| p_{cs} | 2 | kW/kg |
| η_{cs} | 0.99 | — |
| p_{ts} | 7 | kW/kg |
| p_{gen} | 13.5 | kW/kg |
| η_{gen} | 0.95 | — |
| p_{ic} | 16.4 | kW/kg |
| η_{ic} | 0.98 | — |

The assumptions at the technological level are made to consider the 2035 technology horizon. In the literature, there is a large uncertainty concerning the future technology perspectives [1,32,70,82,83]^[11]: mostly related to battery parameters. Table 6 reports the assumptions considered here, which correspond to the previous work of Sgueglia et al. [32].

B. Aircraft Optimization with Respect to Fuel and Energy Consumption

In this section, single-objective optimizations are presented. Table 7 reports the setup used: the optimization solver is SNOPT [84], which is a gradient-based algorithm based on the least-squared method.

The nonlinear and linear solvers are block nonlinear Gauss–Seidel and lower-upper (LU) decomposition, respectively. Specifically, the first is used to solve iterative systems and the second to obtain solution for the linearized derivative system. The problem is not scaled, and so the tolerance must be an absolute tolerance.

One issue regarding the gradient methods is that the optimum point \mathbf{x}^* can be a local minimum; to increase the likelihood of convergence to the global optimum, a multistart check is performed with 10 different initial vectors $\mathbf{x}^{(0)}$. The starting points are generated using the Latin hypercube sampling technique [85] in order to have them spaced within the design space reported in Table 4.

As an example, Table 8 reports the final objective function $f^* = E_c^*$ and the norm of constraints in the case of a hybrid aircraft with 32 engines, designed for a range of 900 n miles; for brevity, only this case is reported, and the others are similar in nature. From Table 8, no evidence of local minima is detected since the maximum difference among the 10 values of f^* is less of 0.4%.

Table 7 Optimization setup for the hybrid aircraft design problem using gradient-based method

| Parameter | Value |
|------------------------|---------------------|
| Optimization solver | SNOPT |
| Linear solver | Linear Gauss–Seidel |
| Nonlinear solver | Direct solver |
| MDA tolerance | 10^{-6} |
| Optimization tolerance | 10^{-6} |

The aircraft have been optimized considering both fuel and energy consumption. A total of four different configurations are considered: three hybrid-electric aircraft, varying the number of engines from 16 to 48, and a conventional configuration; each of them is sized on four different range values equally spaced from 600 to 1500 n miles. Figures 7 and 8 show the fuel and energy consumption with respect to range for each configuration; as a complement to these plots, Tables 9–12 report the quantities of interest for the conventional aircraft and the hybrid aircraft with 16, 32, and 48 engines, respectively.

First result to highlight is that the configuration that optimizes the fuel consumption corresponds to the configuration that minimized the energy consumption, which is intuitive since these parameters are correlated each other.

From Figs. 7 and 8, a point of breakdown in the design range is detected, in agreement with the previous results from Sgueglia et al. [32]. The hybrid aircraft is significantly heavier than the reference aircraft, and it has worse performance in cruise. The zone of interest for its design is limited to short range because, in this region, the benefits overcome the penalties due to the greater mass in cruise because they come from a fully electric climb, which translates in about 2 t of fuel saved. On longer ranges, the mass introduced by batteries diverges, making the concept a poor performer against a conventional aircraft; also, it is worth noting that, due to the divergence, it is not possible to get any feasible aircraft above $R = 1600$ n miles.

The preceding results show that, in the zone of interest for design, the best performing configuration corresponds to $N_{EM} = 32$. The $N_{EM} = 16$ case shows the best aerodynamics’ performance, with a maximum lift-over-drag (LOD) around 18.05 because it has less wetted area due to the lower number of engines. Despite that, the propulsion is poorly distributed, and to satisfy the constraint on fan dimension, the FPR needs to be augmented (around 1.3 from Table 10), worsening the propulsive efficiency.

The opposite case, with highly distributed propulsion ($N_{EM} = 48$), does not show more promising results. Thanks to the large number of engines, the fan size is not limited by the constraint on their dimension; but, since the space over the wing is limited by the span, the FPR is increased in any case to satisfy allocation. Moreover, it has more wetted surfaces and the aerodynamics is significantly worsened. The combination of these two effects makes this configuration worse than the others.

The case $N_{EM} = 32$ represents a balance between aerodynamics and propulsive efficiency: the maximum lift-to-drag ratio is only 1.3% lower than the case with 16 engines, but the FPR is significantly lower (around 1.1 from Table 11), resulting in good aerodynamics and propulsion. As a consequence, the battery volume is lower for this configuration than the others, for all the ranges, which limits the increase in mass. The MTOW and OEW are greater in any case due to the higher number of elements present in the architecture. Nonetheless, even for the best performing configuration, the zone of interest is still limited: regarding the fuel consumption, the design zone is limited to 1500 n miles, whereas regarding the energy consumption it is limited to 900 n miles.

Analysing the certification constraints, it can be noted that all the configurations comply with the revised CS-25 [76]; also, results from Tables 10–12 show that the most stringent condition is the CS-25.121 (b) [76], related to the climb rate at 400 ft of altitude and in the OCI case.

^[11]Delhaye, J., “Electrical Technologies for Aviation of the Future,” Airbus, 2015, <https://ec.europa.eu/research/index.cfm?pg=events&eventcode=E6B592A3-C341-5F62-B5950B69BFB6824D.=2015> [retrieved 09 May 2020].

Table 8 Final objective function $f^* = E_c^*$ and norm of constraints for the 10 optimization runs carried out for hybrid aircraft featuring DEP, $N_{EM} = 32$, and $R = 900$ n miles^a

| | Run | | | | | | | | | |
|---------|---------|---------|---------|-----------|---------|---------|---------|---------|---------|---------|
| | 1 | 2 | 3 | 4 | 5 | 6 | 7 | 8 | 9 | 10 |
| f^* | 255,246 | 255,259 | 255,231 | 2,552,283 | 255,242 | 255,219 | 255,220 | 255,236 | 255,218 | 255,262 |
| $\ c\ $ | 0 | 0 | 0 | 0 | 0 | 0 | 0 | 0 | 0 | 0 |

^aThe best value obtained is $x^* = 255218$.

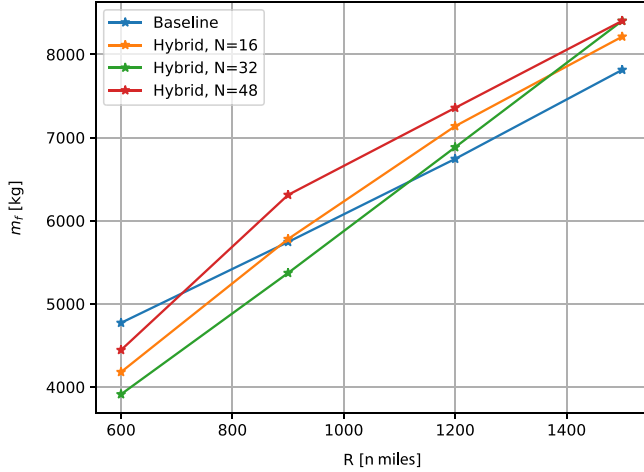


Fig. 7 Fuel consumption vs range plot for three different hybrid-electric configurations ($N_{EM} = 16, 32, 48$) and conventional aircraft with the same TLARs: EIS = 2035.

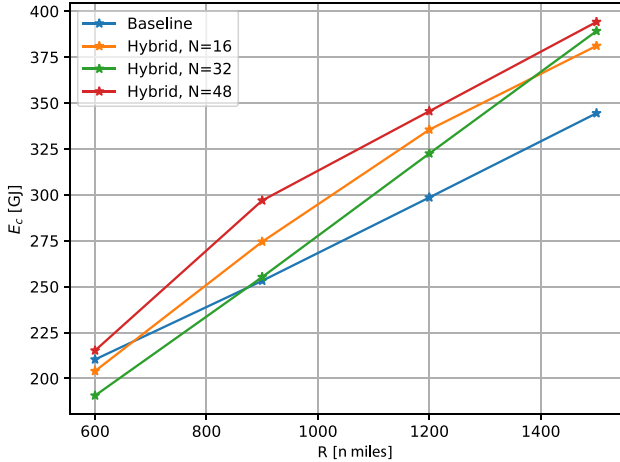


Fig. 8 Energy consumption vs range plot for three different hybrid-electric configurations ($N_{EM} = 16, 32, 48$) and conventional aircraft with the same TLARs: EIS = 2035.

In conclusion, there is an agreement between the fuel and energy consumption trend with respect to design range both for optimized and nonoptimized configuration [32], but the allowable region is slightly increased. The average computational time is 35 min per simulation, and 30–40 iterations are required to reach the convergence.

C. Pareto Front Using Gradient Information

Multiobjective optimization is performed using the OEW and E_c as objectives to reduce both structural weight and energy consumption, as well as compute a Pareto front. Both quantities have effects on costs, and thus this optimization can give some indications on the points that optimize costs. OEW is preferred to MTOW because the latter depends directly on fuel (whereas OEW is affected only indirectly), and results can be misleading [44]. Two optimization packages are used: NSGA-II [86] and SNOPT [84]. NSGA-II is a genetic

Table 9 Quantities of interest for the reference aircraft results: A320 type resized to match EIS = 2035

| | Range, n miles | | | |
|---------------------------------|----------------|--------|--------|--------|
| | 600 | 900 | 1200 | 1500 |
| MTOW, t | 56.76 | 57.89 | 59.01 | 60.14 |
| OEW, t | 38.58 | 38.71 | 38.79 | 38.84 |
| Wing area, m^2 | 116.21 | 116.47 | 116.63 | 116.76 |
| Maximum LOD | 18.47 | 18.46 | 18.45 | 18.44 |
| Fuel mission, t | 4.77 | 5.74 | 6.77 | 7.81 |
| CAT.POL.A.410(a)-1 [77], ft/min | 905.76 | 905.59 | 904.13 | 904.48 |
| CAT.POL.A.410(a)-2 [77], ft/min | 308.9 | 315.24 | 309.41 | 300.24 |
| CS-25.119(a) [76], % | 17.54 | 17.61 | 17.57 | 17.49 |
| CS-25.121(a) [76], % | 4.5 | 4.29 | 4.02 | 3.62 |
| CS-25.121(b) [76], % | 6.37 | 6.14 | 5.9 | 5.47 |
| CS-25.121(c) [76], % | 6.86 | 6.72 | 6.51 | 6.28 |
| CS-25.121(d) [76], % | 7.01 | 7.03 | 6.99 | 6.93 |

Table 10 Quantities of interest for the optimized hybrid aircraft with distributed electric ducted fan: $N_{EM} = 16$

| | Range, n miles | | | |
|---------------------------------|----------------|---------|---------|---------|
| | 600 | 900 | 1200 | 1500 |
| MTOW, t | 72.8 | 74.4 | 75.8 | 77.6 |
| OEW, t | 55.4 | 55.5 | 4504 | 56.6 |
| Wing area, m^2 | 104.26 | 106.71 | 108.18 | 110.28 |
| Maximum LOD | 18.05 | 18.03 | 18.04 | 18.03 |
| Battery volume, m^3 | 1.56 | 1.67 | 1.86 | 1.94 |
| FPR | 1.26 | 1.28 | 1.28 | 1.29 |
| Fuel mission, t | 4.18 | 5.78 | 7.14 | 8.21 |
| Energy consumption, GJ | 204.03 | 274.47 | 335.50 | 381.13 |
| CAT.POL.A.410(a)-1 [77], ft/min | 1438.64 | 1355.65 | 1324.17 | 1193.95 |
| CAT.POL.A.410(a)-2 [77], ft/min | 1312.39 | 1310.58 | 1648.61 | 1307.07 |
| CS-25.119(a) [76], % | 12.27 | 12.25 | 12.09 | 12.21 |
| CS-25.121(a) [76], % | 24.02 | 24.76 | 24.57 | 24.2 |
| CS-25.121(b) [76], % | 2.41 | 2.46 | 2.51 | 2.76 |
| CS-25.121(c) [76], % | 24.10 | 23.73 | 23.23 | 23.14 |
| CS-25.121(d) [76], % | 10.80 | 10.80 | 10.65 | 10.76 |

algorithm that explores a large number of prescribed points and automatically computes the sets of optimal points belonging to the Pareto frontier.

SNOPT only solves single-objective problems, and so a composite function that depends on OEW and E_c is defined:

$$f(x, \alpha) = \alpha \frac{OEW}{OEW_{ref}} + (1 - \alpha) \frac{E_c}{E_{c,ref}} \quad (11)$$

where $\alpha \in [0, 1]$ is varied to obtain the Pareto front. The two quantities are nondimensionalized with respect to reference values.

Just one configuration is considered, corresponding to $N_{EM} = 32$ and $R = 900$ n miles. The exploration process done by the genetic algorithm is shown in Fig. 9: 20,000 points were explored, marked in green; then, between all these points, it finds the feasible ones that satisfy the design constraints and finally gets all the nondominated

Table 11 Quantities of interest for the optimized hybrid aircraft with distributed electric ducted fan: $N_{EM} = 32$

| | Range, n miles | | | |
|--------------------------------|----------------|---------|---------|---------|
| | 600 | 900 | 1200 | 1500 |
| MTOW, t | 77.7 | 78.4 | 70.1 | 80.4 |
| OEW, t | 59.9 | 60.3 | 60.9 | 61.3 |
| Wing area, m^2 | 119.89 | 121.26 | 124.26 | 128.42 |
| Maximum LOD | 17.81 | 17.82 | 17.81 | 17.81 |
| Battery volume, m^3 | 1.55 | 1.67 | 1.72 | 1.92 |
| FPR | 1.12 | 1.12 | 1.12 | 1.13 |
| Fuel mission, t | 3.91 | 5.37 | 6.88 | 8.39 |
| Energy consumption, GJ | 190.67 | 255.24 | 322.52 | 389.20 |
| CAT.POLA.410(a)-1 [77], ft/min | 1125.10 | 1175.56 | 1142.56 | 1058.09 |
| CAT.POLA.410(a)-2 [77], ft/min | 1209.61 | 1267.16 | 12607 | 1135.13 |
| CS-25.119(a) [76], % | 11.25 | 11.62 | 11.61 | 11.60 |
| CS-25.121(a) [76], % | 24.59 | 24.29 | 24.29 | 22.74 |
| CS-25.121(b) [76], % | 2.40 | 2.41 | 2.51 | 2.52 |
| CS-25.121(c) [76], % | 23.46 | 23.18 | 23.18 | 21.81 |
| CS-25.121(d) [76], % | 9.79 | 10.14 | 10.14 | 10.15 |

Table 12 Quantities of interest for the optimized hybrid aircraft with distributed electric ducted fan: $N_{EM} = 48$

| | Range, n miles | | | |
|--------------------------------|----------------|---------|---------|---------|
| | 600 | 900 | 1200 | 1500 |
| MTOW, t | 80.5 | 82.4 | 84.1 | 83.9 |
| OEW, t | 62.5 | 63.9 | 64.7 | 64.2 |
| Wing area, m^2 | 118.26 | 124.12 | 129.1 | 124.08 |
| Maximum LOD | 17.49 | 17.47 | 17.47 | 17.45 |
| Battery volume, m^3 | 1.67 | 1.92 | 2.13 | 2.21 |
| FPR | 1.34 | 1.34 | 1.35 | 1.37 |
| Fuel mission, t | 4.45 | 6.31 | 7.36 | 8.40 |
| Energy consumption, GJ | 215.22 | 296.92 | 345.54 | 394.16 |
| CAT.POLA.410(a)-1 [77], ft/min | 950.35 | 1028.93 | 790.61 | 876.07 |
| CAT.POLA.410(a)-2 [77], ft/min | 1143.42 | 1233.99 | 1063.84 | 1228.31 |
| CS-25.119(a) [76], % | 10.78 | 11.01 | 10.78 | 10.97 |
| CS-25.121(a) [76], % | 22.75 | 22.75 | 22.27 | 22.68 |
| CS-25.121(b) [76], % | 2.61 | 2.52 | 2.84 | 2.58 |
| CS-25.121(c) [76], % | 21.80 | 21.86 | 21.13 | 21.20 |
| CS-25.121(d) [76], % | 9.36 | 9.52 | 9.38 | 9.48 |

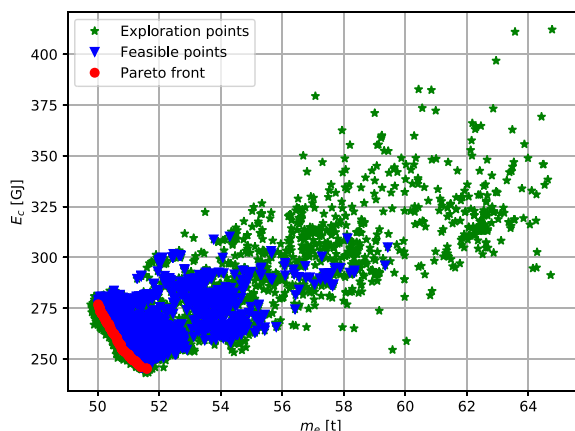


Fig. 9 NSGA-II exploration points to find the Pareto front with respect to OEW and E_c , $N = 32$, and $R = 900$ n miles. Exploration, feasible, and optimal points are marked in green, blue, and red, respectively.

points belonging to the Pareto front. The number of points is chosen in order to obtain a smooth Pareto front; preliminary results showed that, with 10,000 or 15,000, the front was not adequately smooth.

Figure 10 shows the comparison between SNOPT and NSGA-II: visually, it emerges that the two methods are comparable. To better

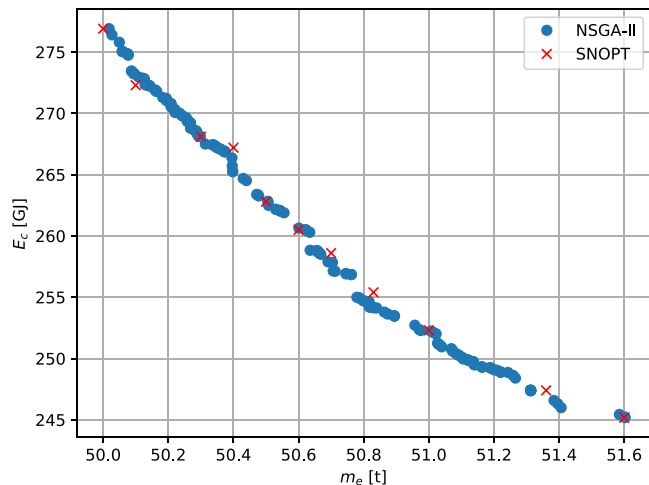


Fig. 10 Pareto front with respect to OEW and E_c : comparison between genetic algorithm NSGA-II and gradient-based solver SNOPT, with $N_{EM} = 32$ and $R = 900$ n miles.

Table 13 \mathcal{L}_2 -norm calculation to compare the two optimizers in terms of optimal objective value f^* and design variables vector x^{*a}

| Parameter | Value |
|-------------------------------------|-----------------------|
| $\ f_{SNOPT}^* - f_{NSGA-II}^*\ _2$ | 2.98×10^{-5} |
| $\ x_{SNOPT}^* - x_{NSGA-II}^*\ _2$ | 1.52×10^{-4} |

^aThe subscript identifies the method.

Table 14 Comparison between design variables of three different configurations, chosen from the Pareto front computed using SNOPT and corresponding to $\alpha = 0$, $\alpha = 0.5$, and $\alpha = 1.0^a$

| | $\alpha = 0$ | $\alpha = 0.5$ | $\alpha = 1$ |
|------------------|--------------|----------------|--------------|
| OEW, t | 62.48 | 61.62 | 60.89 |
| E_c , GJ | 255.24 | 304.09 | 326.19 |
| AR_w | 10.82 | 8.82 | 8.01 |
| S_w , m^2 | 122.41 | 118.9 | 117.22 |
| τ_b , m^2 | 1.67 | 1.69 | 1.72 |

^aEleven values of α are considered for the SNOPT optimization in Eq. (11).

assess the difference between them, the \mathcal{L}_2 -norm [87] is computed for the final objective function value f^* and the design variables vector x^* in the points in which both the SNOPT and NSGA-II results are available. Table 13 reports the values: the difference between the two solutions is lower than 10^{-3} , and thus it is concluded that the two methods lead to same result, although there is still a small difference due to numerical approximation that can be neglected.

Nevertheless, NSGA-II takes about 35 h to get the result; meanwhile, using SNOPT, each point is obtained in around 30 min, for a total of 12 h: with gradient information, the computational cost is reduced by about 70%.

As expected, when the energy decreases, the OEW increases since the optimizer uses mainly the aspect ratio to reduce the energy, which increases the wing weight. However, comparing the design variables' values for three different configurations [corresponding to $\alpha = 0$, $\alpha = 0.5$, and $\alpha = 1$ in Eq. (11), as shown in Table 14], the same behavior does not apply to the battery volume. Since they strongly affect the weight, it is expected that their volume is lower when the OEW is the driven objective. In reality, this is not the case because there are two opposite effects: the reduction in weight, which is beneficial; and the worsening of aerodynamics due to the reduction

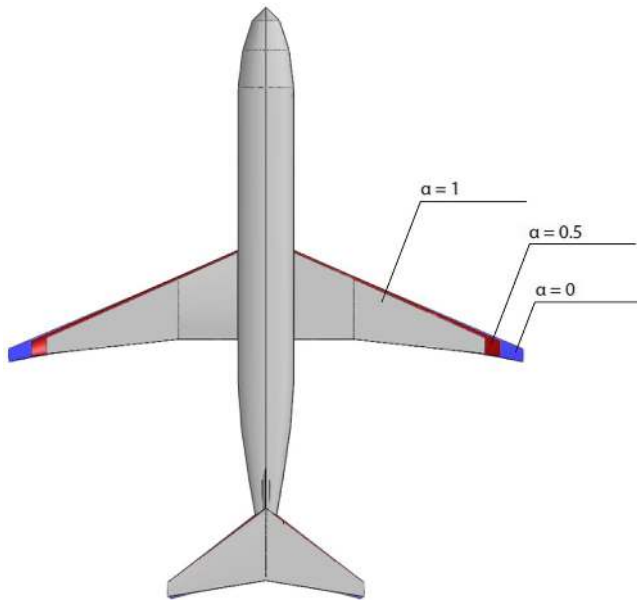


Fig. 11 Comparison between three different configurations, chosen from the Pareto front [see Eq. (11)].

of aspect ratio, which is negative. Between the two, the most dominant effect is the second one, resulting in a larger energy consumption. As a consequence, to satisfy the energy constraint, batteries show a larger battery volume.

A difference is also shown in Fig. 11, in which the three configurations are overlapped. The tails present very small differences, and the major changes of interest are in the wing, where span increases.

V. Conclusions

This work addresses the problem of designing a hybrid-electric aircraft. In particular, the scope is to define an overall conceptual design procedure to deal with this unconventional configuration. The resulting sizing loop relies on the already existing models available in literature that have been expanded and integrated in a design framework. An approach based on MDO techniques is defined to take advantage of its features, such as the possibility to capture all the possible interaction between disciplines: a key point for unconventional configurations that cannot be considered with classical handbook methods.

This goal has been achieved through the integration of the sizing tool FAST and OpenMDAO, which is an open-source optimization tool. The resulting design process relies on analytic derivatives to improve the computational efficiency. The advantages of this framework, mainly related to reduced computational cost, are highlighted. Then, the capability of this code is demonstrated by considering the test case of hybrid aircraft featuring distributed electric ducted fans. Three configurations are considered (16, 32, and 48 electric motors), assuming key technological parameters based on a previous study.

Optimization results show that the hybrid-electric concept is advantageous in a limited region with respect to design range. Specifically, the concept is better performing against a conventional configuration for short ranges, where the possibility to have a fully electric segment counterbalances the increase in weight due to the electric components. For longer distances, the benefits of hybrid propulsion are less important and, finally, a range where the hybrid-electric and the conventional aircraft have the same performance appears. This is defined as breakdown range and, of course, changes with the configuration. After this point, the penalties in weight become more and more relevant and the conventional aircraft shows better performance.

Both fuel and energy consumption are used as objective functions, and it is found that the fuel consumption may be misleading since it does not consider the contribution of batteries, which is purely energy. The latter is more relevant from a design point of view for a dual-energy-source aircraft. Among the configurations studied, it emerges that the case with 32 engines performs well in the zone of

interest for design. This case represents a compromise between aerodynamics and propulsive efficiency. The case with 16 engines is poorly distributed and the FPR is higher in order to not exceed the fan size limit, resulting in a low propulsive efficiency. On the other side, the case with 48 engines requires one to reduce FPR to locate all the motors on the wing; moreover, it shows more wetted area, and thus it is the worst in terms of aerodynamics.

Finally, a Pareto front is obtained using two optimization methods: a genetic algorithm and a gradient-based method. The aircraft empty mass and energy consumption are the parameters selected for the multiobjective optimization. Results of the two methods are comparable to each other, but the gradient-based method produces results faster than the genetic algorithm; in particular, the reduction in computational time is approximately 70%.

Overall, the capability of the MDO framework to deal with the hybrid-electric aircraft design problem has been demonstrated. The possibility to capture interactions between disciplines enables exploration of a large design space and trade studies. As a next step, other unconventional configurations, such as the blended wing-body, can be investigated to take advantage of this MDO framework.

Acknowledgments

The authors would like to thank 1) Airbus for the financial support in the frame of Chair for Eco Design of Aircraft; 2) the European Commission for the financial support within the frame of the Joint Technology Initiative Clean Sky 2, Large Passenger Aircraft Innovative Aircraft Demonstration Platform (contract No. CSJU-CS2-GAM-LPA-2014-2015-01); 3) the Formation Doctorale of ISAE-SUPAERO for its financial support and the University of Michigan for having hosted the first author from January to April 2018; and 4) Michael Ridel and David Donjat for their contribution on electric architecture modeling.

References

- [1] Brelje, B. J., and Martins, J. R. R. A., "Electric, Hybrid, and Turboelectric Fixed-Wing Aircraft: A Review of Concepts, Models, and Design Approaches," *Progress in Aerospace Sciences*, Vol. 104, Jan. 2019, pp. 1–19. <https://doi.org/10.1016/j.paerosci.2018.06.004>
- [2] Kirner, R., "An Investigation into the Benefits of Distributed Propulsion on Advanced Aircraft Configurations," Ph.D. Thesis, Cranfield Univ., Cranfield, England, U.K., 2015.
- [3] Gohardani, A. S., Doulgeris, G., and Singh, R., "Challenges of Future Aircraft Propulsion: A Review of Distributed Propulsion Technology and its Potential Application for the all Electric Commercial Aircraft," *Progress in Aerospace Sciences*, Vol. 47, No. 5, 2011, pp. 369–391. <https://doi.org/10.1016/j.paerosci.2010.09.001>
- [4] Smith, L. H., Jr., "Wake Ingestion Propulsion Benefit," *Journal of Propulsion and Power*, Vol. 9, No. 1, 1993, pp. 74–82. <https://doi.org/10.2514/3.11487>
- [5] Peijian, L., Rao, A. G., Ragni, D., and Veldhuis, L., "Performance Analysis of Wake and Boundary-Layer Ingestion for Aircraft Design," *Journal of Aircraft*, Vol. 53, No. 5, 2016, pp. 1517–1526. <https://doi.org/10.2514/1.C033395>
- [6] Schmollgruber, P., Döll, C., Hermetz, J., Liaboeuf, R., Ridel, M., Cafarelli, I., Atinaut, O., François, C., and Paluch, B., "Multidisciplinary Exploration of DRAGON: An ONERA Hybrid Electric Distributed Propulsion Concept," *AIAA SciTech Forum*, AIAA Paper 2019-1585, 2019. <https://doi.org/10.2514/6.2019-1585>
- [7] Ko, A., Schetz, J. A., and Mason, W. H., "Assessment of the Potential Advantages of Distributed Propulsion for Aircraft," *16th International Society for Air Breathing Engines (2003)*, ISABE, Cleveland, OH, 2003, pp. 1–9.
- [8] Borer, N. K., Patterson, M. D., Viken, K. V., Moore, M. D., Bevirt, J., Stroll, A. M., and Gibson, A. R., "Design and Performance of the NASA SCEPTOR Distributed Electric Propulsion Flight Demonstrator," *AIAA Aviation Technology, Integration, and Operations Conference*, AIAA Paper 2016-3920, 2016. <https://doi.org/10.2514/6.2016-3920>
- [9] Clarke, S., Redifer, M., Papatthakis, K. V., Samnuel, A., and Foster, T., "X-57 Power and Command System Design," *2017 IEEE Transportation and Electrification Conference and Expo ITEC*, IEEE Publ., Piscataway, NJ, 2017, pp. 393–400. <https://doi.org/10.1109/ITEC.2017.7993303>

- [10] Deere, K. A., Viken, J. K., Viken, S. A., Carter, M. B., Wiese, M. R., and Farr, N., "Computational Analysis of a Wing Designed for the X-57 Distributed Electric Propulsion Aircraft," *17th AIAA Aviation Technology, Integration, and Operations Conference*, AIAA Paper 2017-3923, 2017.
- [11] Deere, K. A., Viken, J. K., Viken, S. A., Carter, M. B., Wiese, M. R., and Farr, N., "Computational Analysis of Powered Lift Augmentation for the LEAPTech Distributed Electric Propulsion Wing," *35th AIAA Applied Aerodynamics Conference*, AIAA Paper 2017-3921, 2017. <https://doi.org/10.2514/6.2017-3921>
- [12] Schnulo, S. L., Chin, J., Smith, A. D., and Dubois, A., "Steady State Thermal Analyses of SCEPTOR X-57 Wingtip Propulsion," *17th AIAA Aviation Technology, Integration and Operations Conference*, AIAA Paper 2017-3788, 2017. <https://doi.org/10.2514/6.2017-3788>
- [13] Hwang, J. T., and Ning, A., "Large-Scale Multidisciplinary Optimization of an Electric Aircraft for On-Demand Mobility," *AIAA/ASCE/AHS/ASC Structures, Structural Dynamics, and Materials Conference*, AIAA Paper 2018-1384, 2018, pp. 1–18. <https://doi.org/10.2514/6.2018-1384>
- [14] Kim, H. D., Brown, G. V., and Felder, J. L., "Distributed Turboelectric Propulsion for Hybrid Wing Body Aircraft," *2008 International Powered Lift Conference*, Royal Aeronautic Soc., London, 2008.
- [15] Kim, H. D., Felder, J. L., Tong, M. T., Berton, J. J., and Haller, W., "Turboelectric Distributed Propulsion Benefits on the N3-X Vehicle," *Aircraft Engineering and Aerospace Technology*, Vol. 86, No. 6, 2014, pp. 558–561. <https://doi.org/10.1108/AEAT-04-2014-0037>
- [16] Brown, G. V., "Weights and Efficiencies of Electric Components of a Turboelectric Aircraft Propulsion System," *49th AIAA Aerospace Sciences Meeting*, AIAA Paper 2011-0255, 2011. <https://doi.org/10.2514/6.2011-255>
- [17] Felder, J. L., Tong, M. T., and Chu, J., "Sensitivity of Mission Energy Consumption to Turboelectric Distributed Propulsion Design Assumptions on the N3-X Hybrid Wing Body Aircraft," *48th AIAA/ASME/SAE/ASEE Joint Propulsion Conference*, AIAA Paper 2012-3701, 2012.
- [18] Welstead, J., and Felder, J. L., "Conceptual Design of a Single-Aisle Turboelectric Commercial Transport with Fuselage Boundary Layer Ingestion," *54th AIAA Aerospace Sciences Meeting*, AIAA Paper 2016-1027, 2016. <https://doi.org/10.2514/6.2016-1027>
- [19] Welstead, J., Felder, J. L., Guynn, M. D., Haller, W., Tong, M. T., Jones, S., Ordaz, I., Quinlan, J., and Mason, B., "Overview of the NASA STARC-ABL (Rev. B) Advanced Concept," 2017, <https://ntrs.nasa.gov/search.jsp?R=20170005612> [retrieved 04 June 2019].
- [20] Hepperle, M., "Electric Flight—Potential and Limitations," NATO TR STO-MP-AVT-209, Brunswick, Germany, 2012, pp. 1, 30.
- [21] Marwa, M., Martin, S. M., Martos, B. C., and Anderson, R. P., "Analytic and Numeric Forms for the Performance of Propeller-Powered Electric and Hybrid Aircraft," *AIAA Aerospace Sciences Meeting*, AIAA Paper 2017-0211, 2017, pp. 1–37. <https://doi.org/10.2514/6.2017-0211>
- [22] Gray, J. S., Mader, C. A., Kenway, G. K. W., and Martins, J. R. R. A., "Modeling Boundary Layer Ingestion Using a Coupled Aeropropulsive Analysis," *Journal of Aircraft*, Vol. 55, No. 3, 2018, pp. 1191–1199. <https://doi.org/10.2514/1.C034601>
- [23] Schiltgen, B. T., and Freeman, J., "Aeropropulsive Interaction and Thermal System Integration Within the ECO-150: A Turboelectric Distributed Propulsion Airliner with Conventional Electric Machines," *AIAA Aviation Technology, Integration and Operation Conference*, AIAA Paper 2016-4064, 2016. <https://doi.org/10.2514/6.2016-4064>
- [24] Borer, N. K., Derlaga, J. M., Deere, K. A., and Carter, M. B., "Comparison of Aero-Propulsive Performance Predictions for Distributed Propulsion Configurations," *AIAA Aerospace Sciences Meeting*, AIAA Paper 2017-0209, 2017, pp. 1–16. <https://doi.org/10.2514/6.2017-0209>
- [25] Freeman, J., Osterkamp, P., Green, M. W., Gibson, A. R., and Schiltgen, B. T., "Challenges and Opportunities for Electric Aircraft Thermal Management," *Aircraft Engineering and Aerospace Technology*, Vol. 86, No. 6, 2014, pp. 519–524. <https://doi.org/10.1108/AEAT-04-2014-0042>
- [26] Isikveren, A. T., Kaiser, S., Pomet, C., and Vranty, P. C., "Pre-Design Strategies and Sizing Techniques for Dual-Energy Aircraft," *Aircraft Engineering and Aerospace Technology*, Vol. 86, No. 6, 2014, pp. 525–542. <https://doi.org/10.1108/AEAT-08-2014-0122>
- [27] Pomet, C., Seitz, A., Isikveren, A. T., and Hornung, M., "Methodology for Sizing and Performance Assessment of Hybrid Energy Aircraft," *Journal of Aircraft*, Vol. 52, No. 1, 2015, pp. 341–352. <https://doi.org/10.2514/1.C032716>
- [28] Cinar, G., Mavris, D. N., Emeneth, M., Schneegans, A., and Fefermann, Y., "Sizing, Integration and Performance Evaluation of Hybrid Electric Propulsion Subsystem Architectures," *AIAA Aerospace Sciences Meeting*, AIAA Paper 2017-1183, 2017, pp. 1–18. <https://doi.org/10.2514/6.2017-1183>
- [29] Ludowicy, J., Rings, R., Finger, D. F., and Braun, C., "Sizing Studies of Light Aircraft with Serial Hybrid Propulsion Systems," *Deutscher Luft- und Raumfahrtkongress*, DLR, Cologne, Germany, 2018, pp. 1–11. <https://doi.org/10.25967/480226>
- [30] de Vries, R., Hoogreef, M. F. M., and Vos, R., "Preliminary Sizing of a Hybrid-Electric Passenger Aircraft Featuring Over-the-Wing Distributed-Propulsion," *AIAA SciTech Forum*, AIAA Paper 2019-1811, 2019. <https://doi.org/10.2514/6.2019-1811>
- [31] de Vries, R., Brown, M., and Vos, R., "Preliminary Sizing Method for Hybrid-Electric Distributed-Propulsion Aircraft," *Journal of Aircraft*, Vol. 56, No. 6, 2019, pp. 2172–2188. <https://doi.org/10.2514/1.C035388>
- [32] Sgueglia, A., Schmollgruber, P., Bartoli, N., Atinault, O., Benard, N., and Morlier, J., "Exploration and Sizing of a Large Passenger Aircraft with Distributed Electric Ducted Fans," *AIAA SciTech Forum*, AIAA Paper 2018-1745, 2018, pp. 1–33. <https://doi.org/10.2514/6.2018-1745>
- [33] Sgueglia, A., "Methodology for Sizing and Optimising a Blended Wing-Body with Distributed Electric Ducted Fans," Ph.D. Thesis, National Higher French Institute of Aeronautics and Space, Toulouse, France, 2019.
- [34] Martins, J. R. R. A., and Lambe, A. B., "Multidisciplinary Design Optimization: A Survey of Architectures," *AIAA Journal*, Vol. 51, No. 9, 2013, pp. 2049–2075. <https://doi.org/10.2514/1.J051895>
- [35] Brelje, B. J., and Martins, J. R., "Development of a Conceptual Design Model for Aircraft Electric Propulsion with Efficient Gradients," *2018 AIAA/IEEE Electric Aircraft Technologies Symposium*, AIAA Paper 2018-4979, 2018. <https://doi.org/10.2514/6.2018-4979>
- [36] Hwang, J. T., and Ning, A., "Large-Scale Multidisciplinary Optimization of an Electric Aircraft for On-Demand Mobility," *AIAA/ASCE/AHS/ASC Structures, Structural Dynamics, and Materials Conference*, AIAA Paper 2018-1384, 2018, pp. 1–18. <https://doi.org/10.2514/6.2018-1384>
- [37] Antcliff, K. R., Guynn, M. D., Marien, T., Wells, D. P., Schneider, S. J., and Tong, M. J., "Mission Analysis and Aircraft Sizing of a Hybrid-Electric Regional Aircraft," *54th AIAA Aerospace Sciences Meeting*, AIAA Paper 2016-1028, 2016. <https://doi.org/10.2514/6.2016-1028>
- [38] Finger, D. F., Braun, C., and Bil, C., "An Initial Sizing Methodology for Hybrid-Electric Light Aircraft," AIAA Paper 2018-4229, 2018. <https://doi.org/10.2514/6.2018-4229>
- [39] Kim, H. D., Felder, J. L., Tong, M. T., and Armstrong, M. J., "Revolutionary Aeropropulsion Concept for Sustainable Aviation: Turboelectric Distributed Propulsion," *21st International Symposium on Air Breathing Engines (ISABE)*, ISABE, 2013.
- [40] Schmollgruber, P., Bedouet, J., Sgueglia, A., Defoort, S., Lafage, R., Bartoli, N., Gourinat, Y., and Benard, E., "Use of a Certification Constraints Module for Aircraft Design Activities," *AIAA Aviation Forum*, AIAA Paper 2017-3762, 2017, pp. 1–19. <https://doi.org/10.2514/6.2017-3762>
- [41] Gray, J. S., Hwang, J. T., Martins, J. R. R. A., Moore, K. T., and Naylor, B. A., "OpenMDAO: An Open-Source Framework for Multidisciplinary Design, Analysis, and Optimization," *Structural and Multidisciplinary Optimization*, Vol. 59, No. 4, 2019, pp. 1075–1104. <https://doi.org/10.1007/s00158-019-02211-z>
- [42] Hwang, J. T., and Martins, J. R. R. A., "A Computational Architecture for Coupling Heterogeneous Numerical Models and Computing Coupled Derivatives," *ACM Transactions on Mathematical Software*, Vol. 44, No. 4, 2018, pp. 1–39. <https://doi.org/10.1145/3233179>
- [43] Schmollgruber, P., Bartoli, N., Bedouet, J., Benard, E., and Gourinat, Y., "Improvement of the Aircraft Design Process for Air Traffic Management Evaluations," *AIAA SciTech Forum*, AIAA Paper 2018-0283, 2018. <https://doi.org/10.2514/6.2018-0283>
- [44] Schmollgruber, P., "Enhancement of the Aircraft Design Process Through Certification Constraints Management and Full Mission Simulations," Ph.D. Thesis, National Higher French Institute of Aeronautics and Space, Toulouse, France, 2018.
- [45] Bohari, B., Borlon, A., Mendoza Santos, B. P., Sgueglia, A., Benard, E., Bronz, M., and Defoort, S., "Conceptual Design of Distributed Propellers Aircraft: Non-Linear Aerodynamic Model Verification of Propeller-Wing Interaction in High-Lift Configuration," *AIAA SciTech*

- Forum*, AIAA Paper 2018-1742, 2018, pp. 1–27.
<https://doi.org/10.2514/6.2018-1742>
- [46] Sgueglia, A., Schmollgruber, P., Benard, E., Bartoli, N., and Morlier, J., “Preliminary Sizing of a Medium Range Blended Wing-Body Using a Multidisciplinary Design Analysis Approach,” *MATEC Web of Conferences*, Vol. 233, CEAS, 2018, pp. 1–8.
<https://doi.org/10.1051/mateconf/201823300014>
- [47] Sgueglia, A., Schmollgruber, P., Benard, E., Bartoli, N., and Morlier, J., “Exploration and Optimization of a Blended Wing-Body Featuring Distributed Electric Propulsion,” *1st Aerospace European Conference 2020*, 3AF, 2020.
- [48] Jasa, J. P., Hwang, J. T., and Martins, J. R. R. A., “Open-Source Coupled Aerostructural Optimization Using Python,” *Structural and Multidisciplinary Optimization*, Vol. 57, No. 4, 2018, pp. 1815–1827.
<https://doi.org/10.1007/s00158-018-1912-8>
- [49] Chung, H., Hwang, J. T., Gray, J. S., and Kim, H. A., *Topology Optimization in OpenMDAO*, Springer, New York, 2019, pp. 1385–1400.
- [50] Hwang, J. T., Lee, D. Y., Cutler, J. W., and Martins, J. R. R. A., “Large-Scale Multidisciplinary Optimization of a Small Satellite’s Design and Operation,” *Journal of Spacecraft and Rockets*, Vol. 51, No. 5, 2014, pp. 1648–1663.
<https://doi.org/10.2514/1.A32751>
- [51] Hwang, J. T., Jasa, J. P., and Martins, J. R., “High-Fidelity Design-Allocation Optimization of a Commercial Aircraft Maximizing Airline Profit,” *Journal of Aircraft*, Vol. 56, No. 3, 2019, pp. 1164–1178.
- [52] Gray, J. S., and Martins, J. R. R. A., “Coupled Aeropropulsive Design Optimization of a Boundary-Layer Ingestion Propulsor,” *Aeronautical Journal*, Vol. 123, No. 1259, 2019, pp. 121–137.
<https://doi.org/10.1017/aer.2018.120>
- [53] Li, Y., Deng, J., Mu, C., Xing, Z., and Du, K., “Vertical Distribution of CO₂ in the Atmospheric Boundary Layer: Characteristics and Impact of Meteorological Variables,” *Atmospheric Environment*, Vol. 91, July 2014, pp. 110–117.
<https://doi.org/10.1016/j.atmosenv.2014.03.067>
- [54] Wick, A. T., Hooker, J. R., Hardin, C. J., and Zeune, C. H., “Integrated Aerodynamic Benefits of Distributed Propulsion,” *AIAA SciTech Forum*, AIAA Paper 2015-1500, 2015.
<https://doi.org/10.2514/6.2015-1500>
- [55] Armstrong, M. J., Ross, C. A. H., and Blackwelder, M. J., “Trade Studies for NASA N3-X Turboelectric Distributed Propulsion System Electrical Power System Architecture,” *SAE International Journal of Aerospace*, Vol. 5, No. 2, 2012, pp. 325–336.
<https://doi.org/10.4271/2012-01-2163>
- [56] Dillinger, E., Döll, C., Liaboeuf, R., Toussaint, C., Hermetz, J., Verbeke, C., and Ridel, M., “Handling Qualities of ONERA’s Small Business Concept Plane with Distributed Electric Propulsion,” *31st Congress of the International Council of the Aeronautical Sciences*, Belo Horizonte, Brazil, 2018.
- [57] Hermetz, J., Ridel, M., and Döll, C., “Distributed Electric Propulsion for Small Business Aircraft: A Concept-Plane for Key-Technologies Investigations,” *30th Congress of the International Council of the Aeronautical Sciences*, ICAS, 2016, <https://hal.archives-ouvertes.fr/hal-01408988/document>.
- [58] Visse, W. P. J., and Broomhead, M. J., “GSP: A Generic Object-Oriented Gas Turbine Simulation Environment,” National Aerospace Lab. NLR-TP-2000-267, 2000.
- [59] Roskam, J., *Airplane Design Part I: Preliminary Sizing of Airplanes*, 4th ed., DARcorporation, Lawrence, KS, 2005.
- [60] Raymer, D. P., *Aircraft Design: A Conceptual Approach*, 6th ed., AIAA, Reston, VA, 2018.
- [61] Roskam, J., *Airplane Design Part II: Preliminary Configuration Design and Integration of the Propulsive System*, 4th ed., DARcorporation, Lawrence, KS, 2005.
- [62] Roskam, J., *Airplane Design Part III: Layout Design of Cockpit, Fuselage, Wing and Empennage: Cutaways and Inboard Profiles*, 4th ed., DARcorporation, Lawrence, KS, 2005.
- [63] Roskam, J., *Airplane Design Part VI: Preliminary Calculation of Aerodynamic, Thrust and Power Characteristics*, 4th ed., DARcorporation, Lawrence, KS, 2005.
- [64] “Devis de Masse des Avions,” DGA–Direction Général de l’Armement, AIR 2001/D, 1984, https://www.defense.gouv.fr/content/download/99062/959409/catalogue_normes_2016.pdf.
- [65] Phillips, W. F., *Mechanics of Flight*, 2nd ed., Wiley, Hoboken, NJ, 2010.
- [66] Lambe, A. B., and Martins, J. R. R. A., “Extensions to the Design Structure Matrix for the Description of Multidisciplinary Design Analysis and Optimization Processes,” *Structural and Multidisciplinary Design Optimization*, Vol. 46, No. 2, 2012, pp. 273–284.
<https://doi.org/10.1007/s00158-012-0763-y>
- [67] Tremblay, O., and Dessaint, L.-A., “Experimental Validation of a Battery Dynamic Model for EV Applications,” *World Electric Vehicle Journal*, Vol. 3, No. 2, 2009, pp. 289–298.
<https://doi.org/10.3390/wevj3020289>
- [68] Lowry, J., and Larminie, J., *Electric Vehicle Technology Explained*, 2nd ed., Wiley, Hoboken, NJ, 2012.
- [69] *Commercial Aircraft Propulsion and Energy Systems Research: Reducing Global Carbon Emission*, National Academy of Engineering Committee on Propulsion and Energy Systems to Reduce Commercial Aviation Carbon Emissions, National Academies Press, 2016, pp. 51–70.
<https://doi.org/10.17226/23490>
- [70] Belleville, M., “Simple Hybrid Propulsion Model for Hybrid Aircraft Design Space Exploration,” *MEA-More Electric Aircraft Conference*, Toulouse, France, 2015, pp. 1–4, <https://hal.archives-ouvertes.fr/hal-01120080/document>.
- [71] Shaw, J. C., Norman, P., Galloway, S., and Burt, G., “A Method for the Evaluation of the Effectiveness of Turboelectric Distributed Propulsion Power System Architectures,” *SAE International Journal of Aerospace*, Vol. 7, No. 1, 2014, pp. 35–43.
<https://doi.org/10.4271/2014-01-2120>
- [72] Armstrong, M. J., Ross, C. A. H., and Blackwelder, M. J., “Propulsion System Component Considerations for NASA N3-X Turboelectric Distributed Propulsion System,” *SAE International Journal of Aerospace*, Vol. 5, No. 2, 2012, pp. 344–353.
<https://doi.org/10.4271/2012-01-2165>
- [73] Anderson, J., Jr., *Introduction to Flight*, 7th ed., McGraw–Hill, New York, 2012.
- [74] Anderson, J. D., Jr., *Fundamentals of Aerodynamics*, 5th ed., McGraw–Hill, New York, 2011.
- [75] Niță, M., and Scholz, D., “Estimating the Oswald Factor from Basic Aircraft Geometrical Parameters,” *Deutscher Luft- und Raumfahrtkongress 2012*, Document ID 281424, DLR, Cologne, Germany, 2012.
- [76] *Certification Specification for Large Aeroplanes CS-25, Amd. 3*, European Aviation Safety Agency, Cologne, Germany, 2017, pp. 10–14, Chap. 1-B.
- [77] *Commission Regulation (EU) n. 965/2012*, Official Journal of the European Commission, European Aviation Safety Agency, Cologne, Germany, 2012, p. 98, Chap. 4, <https://www.easa.europa.eu/document-library/regulations/commission-regulation-eu-no-9652012>.
- [78] Steiner, H.-J., Vranty, P. C., Gologan, C., Wiczorek, K., Isikveren, A. T., and Hornung, M., “Performance and Sizing of Transport Aircraft Employing Electrically-Powered Distributed Propulsion,” *Deutscher Luft- und Raumfahrtkongress*, DLR, Cologne, Germany, 2012, pp. 1–10.
- [79] Shaw, J. C., Fletcher, S., Norman, P., Galloway, S., and Burt, G., “Failure Analysis of a Turboelectric Distributed Propulsion Aircraft Electrical Network: A Case Study,” *SAE TP 2015-01-2403*, Warrendale, PA, 2015, pp. 1–7.
<https://doi.org/10.4271/2015-01-2403>
- [80] Belotti, P., Kirches, C., Leyffer, S., Linderoth, J., Luedtke, J., and Mahajan, A., “Mixed-Integer Nonlinear Optimization,” *Acta Numerica*, Vol. 22, May 2013, pp. 1–131.
<https://doi.org/10.1017/S0962492913000032>
- [81] de Barros, A. G., and Wirasinghe, S. C., “New Aircraft Characteristics Related to Airport Planning,” *First ATRG Conference*, WCTR, 1997.
- [82] Bradley, M. K., and Drone, C. K., “Subsonic Ultra Green Aircraft Research: Phase II-Volume II-Hybrid Electric Design Exploration,” NASA CR-2015-218704/Volume II, 2015.
- [83] Friedrich, C., and Robertson, P., “Hybrid-Electric Propulsion for Aircraft,” *Journal of Aircraft*, Vol. 52, No. 1, 2015, pp. 176–189.
<https://doi.org/10.2514/1.C032660>
- [84] Gill, P. E., Murray, W., and Saunders, M. A., “SNOPT: An SQP Algorithm for Large-Scale Constrained Optimization,” *SIAM Review*, Vol. 47, No. 1, 2005, pp. 99–131.
<https://doi.org/10.1137/S0036144504446096>
- [85] Sacks, J., Welch, W. J., Mitchell, T. J., and Wynn, H. P., “Design and Analysis of Computer Experiments,” *Statistical Science*, Vol. 4, No. 4, 1989, pp. 409–423.
<https://doi.org/10.1214/ss/1177012413>
- [86] Deb, K., Pratap, A., Agarwal, S., and Meyerivan, T., “A Fast and Elitist Multiobjective Genetic Algorithm: NSGA-II,” *IEEE Transactions on Evolutionary Computation*, Vol. 6, No. 2, 2002, pp. 182–197.
<https://doi.org/10.1109/4235.996017>
- [87] Giagkiozis, I., and Fleming, P. J., “Methods for Multi-Objective Optimization: An Analysis,” *Information Sciences*, Vol. 293, Feb. 2015, pp. 338–350.
<https://doi.org/10.1016/j.ins.2014.08.071>